DOMAINS OF OBSERVABILTY IN THE NEAR-INFRARED

with

HST/NICMOS

and

(ADAPTIVE OPTICS AUGMENTED) LARGE GROUND-BASED TELESCOPES

A summary study solicited by STScI in preparation for HST Cycle 12

Glenn Schneider
Steward Observatory, University of Arizona

With contributions by and consultations with:
Eric Becklin, UCLA
Laird Close, University of Arizona
Don Figer, STScI
James Lloyd, UC, Berkeley
Bruce Macintosh, LLNL
Dean Hines, Steward Observatory
Claire Max, LLNL
Daniel Potter, University of Hawaii
Marcia Rieke, University of Arizona
Nicholas Scoville, Caltech
Rodger Thompson, University of Arizona
Alycia Weinberger, Carnegie Inst. Of Washington
Rogier Windhorst, Arizona State University

ABSTRACT

This report has been prepared at the request of STScI. It is intended to serve as a guide for HST proposers and TAC panel reviewers in evaluating the need for HST/NICMOS to accomplish the scientific goals of programs under consideration in specific observational domains.

In the years since the first incarnation of NICMOS, ground-based technical capabilities in support of challenging astronomical observations have made great strides, notably in the arena of large telescopes augmented with adaptive optics systems. Some programs, which could once only have been attempted from space, might now be possible with suitable instrumentation on such ground-based facilities. Yet, many of these systems are still in there early evolutionary stages and their theoretical potentials as applied to any particular observation is far from assured, and performance is far from repeatable given the temporally variable line-of-sight conditions encountered at ground-based observatories. The delineation between programs best suited for space and ground, and the complementary nature of others has, in some cases, become blurred. In this report, we review the capabilities of HST/NICMOS and the current state-of-the-art of operational AO systems, as applied to astronomical investigations of contemporary import, and suggest areas of suitability and uniqueness for each where applicable.

CONTENTS / EXECUTIVE SUMMARY

INTRODUCTION
ABSTRACT
CONTENTS / EXECUTIVE SUMMARY

I **SPACE & GROUND**

I.I **HST/NICMOS & ADAPTIVE OPTICS**

I.2 **NICMOS OVERVIEW**
High-level review of NICMOS instrument concept and science goals.

I.2.1 **Optical Channels**
Description of 3 NICMOS cameras: (1) f/80 11"x11 43mas/pix, (2) f/45 19"x19" 76mas/pix, (3) f/17 52"x52" 200mas/pix.

I.2.2 **Detectors**
Description of 256x256 pixel HgCdTe arrays, readout electronics, and performance.

I.2.3 **Observing Modes**
Overview of observing modes: Deep imaging, Wide-field imaging, Line imaging, High dynamic range imaging, Coronagraphy, Polarimetry, Grism spectrophotometry.

I.3 **ADAPTIVE OPTICS OVERVIEW**
General overview of adaptive optics.

I.3.1 **Control Authority and Atmospherics**
Low and high order AO systems & requirements, r_0, t_0 drivers for near-IR.

I.4 **STREHL RATIO - A Fundamental (But Incomplete) Metric**
Definition and wavelength dependence of Strehl, invariance on HST, variability (instability) on ground-based AO systems.

I.4.1 **NICMOS Strehl Ratios**
98% diffraction-limited Strehl in cameras 1 & 2, 84—87% in camera 3.

I.4.2 **AO Strehl Ratios**
Systemic dependencies. Uncontrolled (and uncontrollable) light in the PSF halo.

I.5 **ADAPTIVE OPTICS LIMITATIONS**
The theoretical potential of an AO system is realized for only a small fraction of targets, regions of the sky, and for only very limited periods of time.

I.5.1 **Isoplanatism**
AO images degrade (Strehl, PSF FWHM and 50%EE) off-axis from wavefront reference guide star limiting the correctable field-of-view.

I.5.2 **Guide Star Brightness**
AO images degrade with guide star brightness. Limits for closed-loop control: V ~ 14 for Shack-Hartmann sensors, V ~ 18 for curvature sensors.

I.5.3 **Natural Guide Star (NGS) Sky Coverage**
Statistically ~ 99% of the sky lacks guide stars of sufficient brightness for isoplanatic AO operability with Shack-Hartmann sensors, and > 90% with curvature sensors.

I.5.4 **Laser Guide Stars (LGS)**
Artificial (laser) guide stars systems are not yet mature (or robust) but can improve sky coverage to 10— 50% (when necessary tip/tilt reference stars are available).

I.5.5 **Seeing**
AO images degrade with seeing conditions. Performance scaling with seeing is discussed.

I.5.6 **Zenith Distance (Airmass)**
AO images degrade with increasing airmass; hour angle, so temporal dependence and declination, so spatial dependence. Performance scaling with airmass is discussed.

I.6 "TYPICAL" STREHLS - The Fallacy of Simplification
AO performance is often characterized by Strehl, but characterizing Strehl is complex and "typical" performance metrics are often not realized. An illustrative study on the variability of Strehl with NGS brightness and target declination is discussed.

I.6.1 AO System Descriptions and Performance Characteristics
Current, advertised as typical, AO performance metrics for CFHT, Keck II, Gemini North, La Sillia, Palomar, Lick, Subaru and VLT UT4 AO systems with facility instruments are summarized.

II SCIENCE CASES AND CONSIDERATIONS
We discuss NICMOS and AO applicability for representative, but diverse, astronomical investigations, and identify the observational domains of uniqueness overlap, and complementary science.

II.1 Sky-Limited Observations: Background vs. Aperture
NICMOS is significantly more sensitive than ground-based telescopes at $\lambda < 1.8$ μm due to very low sky backgrounds (several hundred times lower in H-band). At K-band large AO telescopes have point-source sensitivities competitive with NICMOS.

II.1.1 Faint Galaxies
NICMOS is advantageous because of very low J—H band backgrounds, sharp, repeatable and near perfect Strehl with 110—160 mas spatial resolution, spatial and temporal invariance of its PSF over large (52"x52" FOV), and very large dynamic sampling range.

II.1.1.1 A "Historical Note" of Significance
The importance of very high Strehls and dynamic range is reviewed in the context of WF/PC-1 faint galaxy science with the aberrated HST.

II.1.2 Deep Imaging
NICMOS imaging in the Hubble Deep Field reached 1 σ per-pixel noise levels of AB mag ~ 31.8 in F110W and F160W, in 36.5 h of integration time, with reliable detections of galaxies as faint as AB mag = 30.0 and were not yet approaching the systematic sensitivity limits. Such performance is unmatched from the ground.

II.2 Crowded Field Photometry/Astrometry
We discuss the relative merits of AO and NICMOS observations in optically obscured, but near-IR crowded fields in subsections II.2.1 and II.2.2.

II.2.1 The Arches Cluster
Studies of the mass-function of the Arches Cluster with Gemini/Hokupa'a and NICMOS from H and K band photometry, with comparable spatial resolutions, are reviewed. The Gemini data suffer from incompleteness and probe the mass function to a lower limit of ~ 13 solar masses, compared to 2 solar masses for NICMOS.

II.2.2 The Galactic Center
The highly stable NICMOS PSF enables very accurate multi-color photometry and searches for stellar variability in the crowded region such as the galactic center, and (by example) set an upper limit to the dereddened flux from SgrA*. Paschen α imaging (not possible from the ground) is presented. VLT/NAOS(CONICA) imaging with a currently unique near-IR WFS produced Ks-band images possibly astrometrically superior to NICMOS and significantly improved upon earlier ground-based position measures of the galactic center stars.

II.3 CORONAGRAPHY OF CIRCUMSTELLAR ENVIRONMENTS
NICMOS PSF-subtracted coronagraphy achieves per-pixel H-band background rejection from the PSF wings of an occulted target of 10^7 at r = 1". We discuss the utility of this observing mode for imaging circumstellar debris disks and substellar companions in sections II.3.1 — II.3.3.

II.3.1 Debris Disk Imaging
Spatially resolved imaging of debris disks from the ground is extremely difficult, and in general, AO augmentation provides little or only modest benefits. We illustrate this with comparative ground- and NICMOS imaging of debris disks (sections II.3.1.1, HD 141569A; II.3.1.2, HR 4796A; II.3.1.3, Tw Hya) which were first imaged by, and not particularly challenging for, NICMOS. In section II.3.1.4 we discuss the problem of "false positive" disk detections which have arisen from ground-based imaging.

II.3.2 Polarimetry & High Contrast Imaging: Nulling Polarimetry
Nulling polarimetry on ground-based AO systems provides an avenue for imaging the polarized light component of circumstellar disks. We discuss this method comparatively with NICMOS coronagraphy and Gemini/Hokupa'a nulling polarimetric imaging of the GM Aurigae disk. We also comment on the uniqueness of NICMOS high spatial resolution polarimetry over a wide (19" x 19") fields with embedded targets.

II.3.3 Imaging Brown-Dwarf and Young Jovian Planet Companions
We present results from substellar companion imaging programs with NICMOS coronagraphy and the Keck and Gemini AO systems. On average NICMOS is at least 2 to 5 times more sensitive than Keck in the regions from 0.3" to 1.5" from the star, and delivers highly repeatable performance over the entire sky. In addition, direct comparison of TWA6"B" ($\Delta H = 13.2$ at $r = 2.5$") observations (section II.3.3.1) shows much higher detection sensitivity of NICMOS relative to Keck AO. We also discuss NICMOS non-coronagraphic companion imaging for separations < 0.3" and complementary ground-based AO imaging in this spatial domain.

II.4 High Resolution Broad Band and Line Imaging
For programs where spatial resolution is the primary scientific requirement, large telescopes with AO systems can outperform NICMOS at comparable wavelengths. We illustrate broadband and neutral hydrogen line imaging of the ultraluminous IR galaxy NGC 6240 ,with NICMOS and the Keck II AO system.

SUMMARY

ACKNOWLEDGMENTS

Notes To Readers:

1) This report may be downloaded in PDF, PostScript, or MS Word formats from:
http://nicmosis.as.arizona.edu:8000/REPORTS/NICMOS_AO_WHITEPAPER.html

2) Many of the figures (images and illustrations) in this document are intended for color display and printing. Hard-copies of these figures, if reproduced in black and white (gray scale), may lose their intended conveyance of information.

INTRODUCTION

The Hubble Space Telescope provides a unique enabling platform for near-infrared astronomy, which has been exploited by NICMOS, opening avenues for scientific investigations with high efficiency that remain unmatched by ground-based facilities in many observational domains. Today's large (10 meter class) ground-based telescopes deliver raw light-gathering power exceeding HST's by a factor of twenty, and with augmented technologies such as adaptive optics even smaller telescopes (3-5 meter class) can, under the right conditions, yield superior spatial resolutions. Such facilities are beginning to challenge the observational uniqueness space, which once was wholly in the domain of a space-based instrumental platform (i.e. HST).

Despite the great advances in recent technological achievements implemented at many ground-based facilities, the stability of the HST platform and its atmosphere-free environment giving it unfettered diffraction-limited access over the entire sky and across all accessible wavelengths, continue to make it the facility of choice, and indeed necessity, for many scientific investigations. Understanding when proposed ground-based programs may succeed using new observing technologies, and when would likely fall-short of (if not fail to) achieve their intended goals has become an increasingly complex task. Here we attempt to lend some clarity to this issue by reviewing the capabilities repeatably demonstrated by HST + NICMOS in comparison to those claimed, but achieved with varying degrees of success for particular applications, with the current generation of ground-based facilities.

This report is organized into two principle sections. In section I we provide a brief overview of the NICMOS instrument, its observing modes, and its technical capabilities as integrated with HST and as it is currently being operated by the NICMOS Cooling System. We then provide an overview of Adaptive Optics (AO) technologies as applied to large ground-based telescopes. AO on large-aperture telescopes has been seen as the pathway to enabling observations that at one time could only be considered from space. In doing so we discuss the principle metrics by which AO systems are often evaluated, and the merits of those metrics (which often are inherently unstable) for comparing anticipated performance for actual applications and in light of what has been achieved by HST+NICMOS. In section II we examine results from programs with similar scientific goals and with similar (sometimes identical) targets, as undertaken by HST NICMOS and with large ground-based telescope systems. Here we have drawn *demonstrable results from the published literature*, which are particularly germane in assessing comparative performance in a diversity of observational domains.

I - SPACE & GROUND

I.1 – HST/NICMOS & ADAPTIVE OPTICS

In this section we provide overviews of NICMOS, adaptive optics, fundamental metrics for intercomparison, environmentally and instrumentally imposed limitations on AO systems, and a summary of performance characteristics for currently (or recently) operating AO augmented telescopes and instruments.

I.2 - NICMOS OVERVIEW

After a more than three-year hiatus the Near-Infrared Camera and Multi-Object Spectrometer (NICMOS) was returned to full operational status in HST Cycle 11. The three cameras in the NICMOS instrument provide near-infrared (NIR) imagery with spatial resolutions from ~ 0.1" to 0.25" in spatially adjacent (but non-contiguous) narrow and wide fields-of-view. Working in space in the NIR (from 0.8 – 2.4 μm), NICMOS peers through dusty regions obscured at optical wavelengths that are otherwise compromised by the intrinsic brightness, wavelength-dependent opacity, and turbidity of the Earth's atmosphere. The diversity of instrumental observing modes, including deep-imaging, wide-field imaging, coronagraphy, polarimetry and slitless (grism) spectrophotometry, have allowed NICMOS to address a wide range of astrophysical investigations from within our own solar system to the most distant reaches of the currently observable universe. Emissions from young objects embedded in optically-opaque star and planet forming regions may be studied by NICMOS individually in our own galaxy and collectively in others, and light from the oldest observable galaxies is red-shifted from the rest-frame optical into the NICMOS pass bands.

Originally installed in February 1997, NICMOS was used heavily by astronomers in HST Cycle 7/7N. These capabilities ceased on January 4, 1999 when its supply of solid Nitrogen cryogen, used to cool the instrument detectors and filters, was exhausted. During HST servicing mission 3B (March, 2002) a pathfinder “experiment” in space/cryogenic technology culminated in the subsequent re-cooling and resurrection of NICMOS. With the installation of a reverse Brayton-cycle micro-turbine cooler, heat-exchanger, and external radiator on HST, cryogenic Neon-gas circulating through the NICMOS cooling coils is now maintaining the NICMOS detectors and cold-optics at nearly optimum and highly stable temperatures. NICMOS became the first space cryogenic instrument to ever have been re-activated after cryogen depletion. The success of SM3B has literally moved space infrared (IR) astronomy out of the ice age.

NICMOS extends the Hubble Space Telescope's UV/Optical panchromatic vision into the NIR fulfilling a Level-1 requirement of the HST mission. With NIR light we can see into regions, which are obscured at visible and ultra-violet (UV) wavelengths. Dust, which is pervasive and prevalent in many forms throughout the universe, obscures many of the most interesting objects in optical/UV light and limits our ability to understand the dynamical, evolutionary, and energetic processes in many others. NIR light can penetrate this dust to reveal the birthplaces of planets, stars, and galaxies, as well as the centers of the most powerful galaxies in the universe.

We can also see further back into the ancient history of the universe with NIR light than in the visible and UV. With the global expansion of the universe, electromagnetic radiation is redshifted to longer wavelengths. The intrinsically more distant an object is, the greater the redshift, such that the most distant (currently) observable objects - those with the greatest redshifts - have their optical/UV light redshifted into the infrared. Distant quasars and galaxies provide, in the NIR, a look-back in time to the early epochs of the assemblies of large structures in the universe.

I.2.1 - Optical Channels

NICMOS contains three independently re-imaged optical channels presenting different image scales and field sizes to its NIR detectors over the 0.8–2.4 μm wavelength regime. All three cameras carry nineteen spectral elements, each with sixteen wide, medium-band, and atomic/molecular line filters (~25%, 10%, and 1% pass bands), with a core set of "standard" photometric filters in each camera. Camera 1 provides high-resolution imagery, diffraction limited at and longward of 1μm, over an 11" x 11" field-of-view. This *f*/80 camera is sampled by its focal plane detector with 0.043" pixels. Camera 1 is equipped for polarimetric imaging at 0.8–1.1 μm with < 1% instrumental polarization. Camera 2 provides a wider field (19.3" x 19.4") at *f*/45, and is diffraction limited to a wavelength of 1.75 μm as sampled by 0.076" wide pixels in its image plane. Camera 2 contains coronagraphic optics for high contrast imaging in the regions around point sources, optimized for H-band (1.6 μm) and shorter wavelengths. Instrumentally diffracted and scattered light in the wings of the PSF of coronagraphically occulted targets is reduced significantly when a bright object is placed in the 0.3" radius coronagraphic occulting spot. Imaging polarimetry at wavelengths longer than in camera 1 (1.9 – 2.1 μm) is available in camera 2 with similar low instrumental polarization as in camera 1. Camera 3 enables wide field imaging at "short" wavelengths (< 1.9 μm), with a 52" x 52" field-of-view in its *f*/17 optical channel. Although spatially undersampled with the filters provided, camera 3 is well suited for deep imaging. Camera 3 also provides three grisms for slitless

spectrophotometry, with spectral resolutions of ~ 100, covering the full wavelength range of sensitivity of the NICMOS detectors. The fields-or-view of the three cameras are nearly adjacent on the sky, but not spatially contiguous. Simultaneous imaging with all three cameras is possible, but camera 3 (the "wide field" imager) in not simultaneously confocal with cameras 1 and 2.

I.2.2 - Detectors

NICMOS, the instrument, employs three NICMOS-3/PACE technology detectors, which were manufactured for space-qualified use by the Rockwell Electro-Optics Center under the direction of the University of Arizona's Steward Observatory. The three 256x256 pixel HgCdTe photodiode arrays (one at the re-imaged focal plane of each camera) are indium-bump bonded to a sapphire substrate and addressed through a silicon multiplexor. Each 128 x 128 pixel quadrant is read out through independent on-chip amplifiers (located at the four corners of the focal plane array), and sampled with 16-bit analog-to-digital converters. The NICMOS detectors can be read-out non-destructively while integrating from 0.2 to several thousand seconds, providing a sampling (data quantization) dynamic range of 22 stellar magnitudes in a single exposure. The per-pixel detector read-noise is typically ~ 22 electrons when read-out in this non-destructive "multiaccum" mode. A "bright object mode" supports per-pixel integrations as short as a millisecond. Dark currents are ~ 0.1 e^{-1} s^{-1} $pixel^{-1}$ with the arrays at a temperature of 61K (where they were operated on-orbit from 1997 – 1998 with a solid nitrogen (SN_2) coolant) and ~ 0.2 – 0.3 e^{-1} s^{-1} $pixel^{-1}$ at 77K (where they are currently being operated, cooled by recirculating cold neon gas). The arrays exhibit wavelength-dependent detective quantum efficiencies (dQE) of ~ 30 – 80%, with dQE increasing at longer wavelengths where the inter-pixel dispersion in dQE is greatly reduced. The devices reach hard saturation with well-depths of ~ 200,000 electrons, and respond with a very high degree of linearity to ~ 75% of full well depth.

I.2.3 - Observing Modes

NICMOS opens up many other avenues of scientific investigation through its diversity of observing modes, capabilities and, in cameras 1 and 2, diffraction-limited imaging, such as:

• Deep imaging with very low instrumental plus dark sky backgrounds unmatched from the ground (e.g. 0.024 e^{-1} s^{-1} $pixel^{-1}$ in camera 1's 43 mas x 43 mas pixels).

• Wide-field imaging with camera 3's 52"x52" field-of-view and field-independent point spread function, which is a pathway to uniformly complete and deep imaging surveys.

• Molecular and/or atomic line imaging in bands significantly affected by, or unavailable because of, atmospheric telluric absorption (e.g. Paschen-α at 1.87 μm, a critical tracer of star formation in active galaxies, and typically ~ 30x more efficient than H-α in the optical).

• High dynamic range imaging (e.g. for young exoplanet and circumstellar disk imaging) which, when coupled with Point-Spread-Function (PSF) subtracted coronagraphy, yields per-pixel H-band background rejections in the unocculted wings of the PSF of an occulted point-target of 10^{-7} that of the flux density of the target at a radial distance of 1".

• Polarimetric imaging at high spatial resolution (0.1", critically sampled in camera 1, and 0.2" over a 19.3" x 19.4" field in camera 2), and very low (< 1%) instrumental polarization, which helps elucidate the nature of circumstellar and interstellar grains and their interactions with their environments.

• Full-field low-spectral resolution (R ~ 100) grism (slitless) spectrophotometry at all wavelengths accessible to NICMOS (0.8 – 2.4 μm in three grisms).

NICMOS has no slit or high spectral resolution spectrophotometric capabilities of any kind. Observing programs requiring near-IR high-resolution spectroscopy should look to ground-based facilities and instrumentation (e.g. Keck II/NIRSPEC, VLT/NAOS+CONICA).

I.3. - ADAPTIVE OPTICS OVERVIEW

Adaptive optics systems, in principle, can both correct for static (though temperature and gravity load dependent) wavefront errors in a telescope's optical system and temporally varying image distortions introduced by turbidity in the Earth's atmosphere. The theoretical degree of correction that might be achieved is closely tied to the density (spacing) of actuators used to deform the surface of a corrective optic, and the speed at which corrections can be made. Depending upon the particular system, that dynamically actuated optic might be the telescope's primary or secondary mirror, or a tertiary deformable mirror.

I.3.1 - Control Authority and Atmospherics

"Low-order" AO systems (typically with tens of actuators) deal fairly well with the low-frequency components of static aberrations, but higher order systems (typically with hundreds of actuators and control bandwidths of hundreds of Hz) are required to deal effectively with mid and high frequency components in the static and dynamically degraded wavefront. The size of the wavelength-dependent r_0 seeing circle (i.e., Fried's parameter, the spatial scale of the coherent part of the wavefront) sets a finite limit of the actuator spacings for an AO system. r_0 is typically ~ 20 cm in V band, but is relaxed to 1.2 m in K band under good observing conditions (but must be smaller under turbulent conditions of degraded natural seeing). Ultimately the actuator spacing (and hence number of actuators and the ability of the control system to sense the wavefront, compute the error and nulling terms, and move them at high speed) is limited by the correlation scale length of atmospheric "seeing" cells mapped onto the telescope pupil.

The closed-loop control bandwidth of an AO system must be sufficient to maintain full control authority over the system's actuators and is set, at a minimum, by the wavelength-dependent correlation time, τ_0 (the Greenwood frequency), of the wavefront. In K-band τ_0 is ~ 10 ms from a good site under good conditions, while at V-band a 1.5 ms response would be required,. In practice, however, the correlation time varies significantly with atmospheric conditions. It is for these reasons (coherence time and spatial scales) that AO is currently only practical in the near-IR, and we consider the domains of observability of these systems in light of NICMOS rather than HST's optical and UV instruments.

The ability to partially compensate for the degrading and destructive effects of the Earth's atmosphere by the application of AO technologies has permitted ground-based telescopes to

achieve (or nearly achieve) their theoretical resolution limits. AO systems on 2.5 – 5 meter telescopes are currently in use at Mt. Wilson, Lick Observatory, Mt. Palomar, Calar Alto, ESO (3.6m), Maui (AMOS), UH, and CFHT, the later two using curvature sensing systems. Since resolving power scales with aperture size, 8 – 10 meter class telescopes (e.g. Keck, VLT, GEMINI, SUBARU) when equipped high-order AO correction systems can deliver a four-fold improvement on HST spatial resolution at comparable near-IR wavelengths. For areas of investigation where spatial resolution is of principle concern, a suitably instrumented large ground-based AO augmented system can be effectively used for such programs, and for bright point targets other technologies, such as speckle imaging, may be equally well suited.

I.4 - STREHL RATIO - A Fundamental (But Incomplete) Metric

A metric commonly used to express the potential of a ground-based adaptive optics augmented telescope is the achievable Strehl ratio. Strehl provides a wavelength-dependent measure indicative of the fraction of energy contained in the core of a stellar PSF at the field-point of the AO correction.

In principle, the Strehl ratio is simply the ratio of the peak intensity of the measured PSF to its theoretical maximum. In the absence of instrumental scatter, the Strehl ratio may be approximated as $e^{-(2\pi\sigma_{wfe} / \lambda)^2}$, where σ_{wfe} is the rms wavefront error (from all aberrations) and λ is the wavelength. A theoretical Strehl ratio of 1.0 (or 100%), would imply a perfect optical system with optimal containment of the energy in the PSF. In this definition the Strehl ratio is presumptively static, which is nearly the case for HST, but not so for ground-based AO systems where achievable Strehl ratios exhibit non-random variabilities on many timescales.

I.4.1 - NICMOS Strehl Ratios

For ground-based telescopes Strehl depends (and is limited) in large part upon the natural seeing, air mass (and hence target declination), and guide star brightness. Such effects play no role in degrading HST(+NICMOS)'s diffraction-limited Strehl which is typically ~ 98% in the detector image plane (beyond the Lyot-stop obscured pupil) for cameras 1 and 2 at all wavelengths, and ~ 84% at F110W (roughly J-band) and 87% at F160W (H-band) in Camera 3 as measured from observations in HST cycle 11. The reduction in achievable Strehl ratio for NICMOS camera 3 (relative to cameras 1 and 2) arises because the detector is marginally beyond the range of its internal refocusing mechanism - but is significantly closer to “best focus” than in HST cycle 7. During cycle 7, camera 3 yielded Strehl ratios of ~ 65%, except during two special observing campaigns when the HST secondary mirror was moved to bring the camera into full focal compliance. No such campaigns are planned for cycle 11, as the added benefit now (and presumably for cycle 12 and beyond) would be very small.

I.4.2 - AO Strehl Ratios

The achievable Strehl in AO systems is limited instrumentally by system characteristics such as the actuator density (spacing) on the adaptive mirror, the bandwidth (feedback time constant) of

the control system, the readout (and other) noise in the wavefront sensor and electronics, etc., played against the previously noted dependencies in a complex manner.

While Strehl ratios inform as to how well, instantaneously, an AO system is "peaking up" the light in the core of a target PSF, 1–Strehl indicates how much of the light is uncontrolled. For example a Strehl ratio of 0.3, ("typical" for K-band performance with the Keck AO system with a bright guide star) means that ~ 70% of the stellar light remains in a diffuse halo around the PSF core, and light beyond a fixed angular distance from the PSF core will be fully uncontrolled. AO "correction" provides no benefit in reducing the residual background light in the stellar halo beyond the distance set by Fried's parameter. At near-IR wavelengths on a 10 meter AO augmented telescope, such as the Keck system, this is at angular distances $\geqslant >$ approximately 1.6"

Additionally, Strehl is purely a scalar quantity that provides no information on the temporally variable spatial structure of the light being controlled. Temporal instabilities in PSF structure, not captured in presumptively static Strehl ratios, can be (and usually are), the limiting systematic effects in scientific investigations requiring high levels of background reduction (such as in photometry and astrometry in crowded fields, and debris disk and exoplanet imaging).

I.5 - ADAPTIVE OPTICS LIMITATIONS

Achieving the full theoretical benefit which might be provided by an AO system for any particular target, however, is far from assured and often the full potential of such a system "as advertised" is not realized for many reasons. AO correction requires a wavefront reference (i.e. a "guide star") of sufficient brightness and in close proximity to a target of interest for effective closed-loop (i.e. adaptive atmospheric compensation) correction. The AO control-loop must be closed with sufficient speed, to null out temporally variable changes in the sensed errors in the reference wavefront, but may be (and often is) limited by a variety of contributing noise sources. In practical terms, the theoretical (instrumentally limited) potential of an AO system is realized for only a small fraction of targets, regions of the sky, and for only limited periods of time. We delineate some of the practical limiting factors which constrain AO operations that must be considered in weighing the likely effectiveness of a particular program under consideration as an AO or space experiment, and later elaborate on some of these constraints.

I.5.1 - Isoplanatism

AO correction degrades with angular distance from the wavefront reference (i.e. "guide star"). Typically, AO systems on today's large ground-based telescopes begin to suffer significantly in performance for field-points more than ~ 10" from the guide star. This is not a problem when a program is using the target star as its own reference and the region of interest is only in close proximity to it. Anisoplanatism, however, is a significant problem for large fields and spatially extended targets or extragalactic targets with no bright stars in close proximity. As an example, in Table 1 we show the degradation in Strehl ratio, PSF FWHM, and 50% PSF Energy Encirclement as a function of angular distance from the wavefront sensor star on the Gemini/Hokupa'a system[1] (off-axis:on-axis) under condition of 0.5" natural seeing[2]. Note that Table 1 gives the *degradation* in the Strehl ratio, not the Strehl ratio itself.

In addition to these simple metrics, it should be noted that the structure of the PSF varies in a field-dependent manner, so that post-priori, the PSF of a star in one part of the field cannot be used

---

[1]Hokupa'a is on loan to the Gemini North observatory by the University of Hawaii, but it not currently being offered as a replacement AO system, ALTAIR, is being installed and prepared for commissioning. Expected (but unproven) performance goals for ALTAIR may be found at: http://www.gemini.edu/sciops/instruments/altair/altairIndex.html

[2]http://www.gemini.edu/sciops/instruments/uhaos/uhaosPerfFieldAngle.html

as a template for a star in another part of the field. Anisoplanatism is also wavelength dependent and the isoplanatic angle, to first order, varies as $\lambda^{6/5}$.

TABLE 1: GEMINI/Hokupa'a Field Dependence of Strehl(0.5" seeing)

Wavelength	Strehl/Strehl(0")		FWHM/FWHM(0")		50%EE/50%EE(0")	
(microns)	10"	20"	10"	20"	10"	30"
1.2 (J)	0.6	0.3	1.5	2.4	1.03	1.1
1.6 (H)	0.7	0.4	1.2	1.6	1.1	1.2
2.2 (K)	0.8	0.5	1.1	1.2	1.3	1.4

For NICMOS there is no field dependence in the structure of its PSF or in its ~ 98% Strehl ratios in cameras 1 and 2, and its ~ 86% Strehl ratio achieved over the entire 52" x 52" field-of-view in camera 3.

I.5.2 - Guide Star B

AO correction degrades for fainter guide stars. Wavefront sensors in nearly all AO systems in current operation routinely use optical wavefront sensors, though at several facilities near-IR wavefront correction capability is under development and test, and soon may be in more common use (notably VLT/NAOS). In either case, a reference star used to sense and correct the atmospherically distorted wavefront must be bright enough to provide a non-photon noise limited signal in determining the wavefront correction. For 10-meter class AO systems using a Shack-Hartmann sensor (such as the Keck AO system), AO correction becomes ineffective for guide stars of $V > 14$ (either failing to close the correction loop, or yielding < 1% Strehl so more than 99% of the stellar energy remains uncorrected). Curvature sensors, such as in use on the lower-order Gemini/Hokupa'a system can, under the best of conditions, provide similar corrections for $V < 18$. These metrics indicate where such an AO system provides little, or no, correction and brighter stars are needed to achieve more useful Strehl. To illustrate this, in Figure 1 we reproduce the degradation in on-axis AO performance (Strehl Ratio, FWHM of the stellar PSF, and 50% Encircled Energy) on the Gemini/Hokupa'a system as a function of the AO wavefront sensor's (WFS) guide star R magnitude. The “limiting magnitude” for a guide star is not a fixed quantity, but depends upon both the seeing and the wind speed.

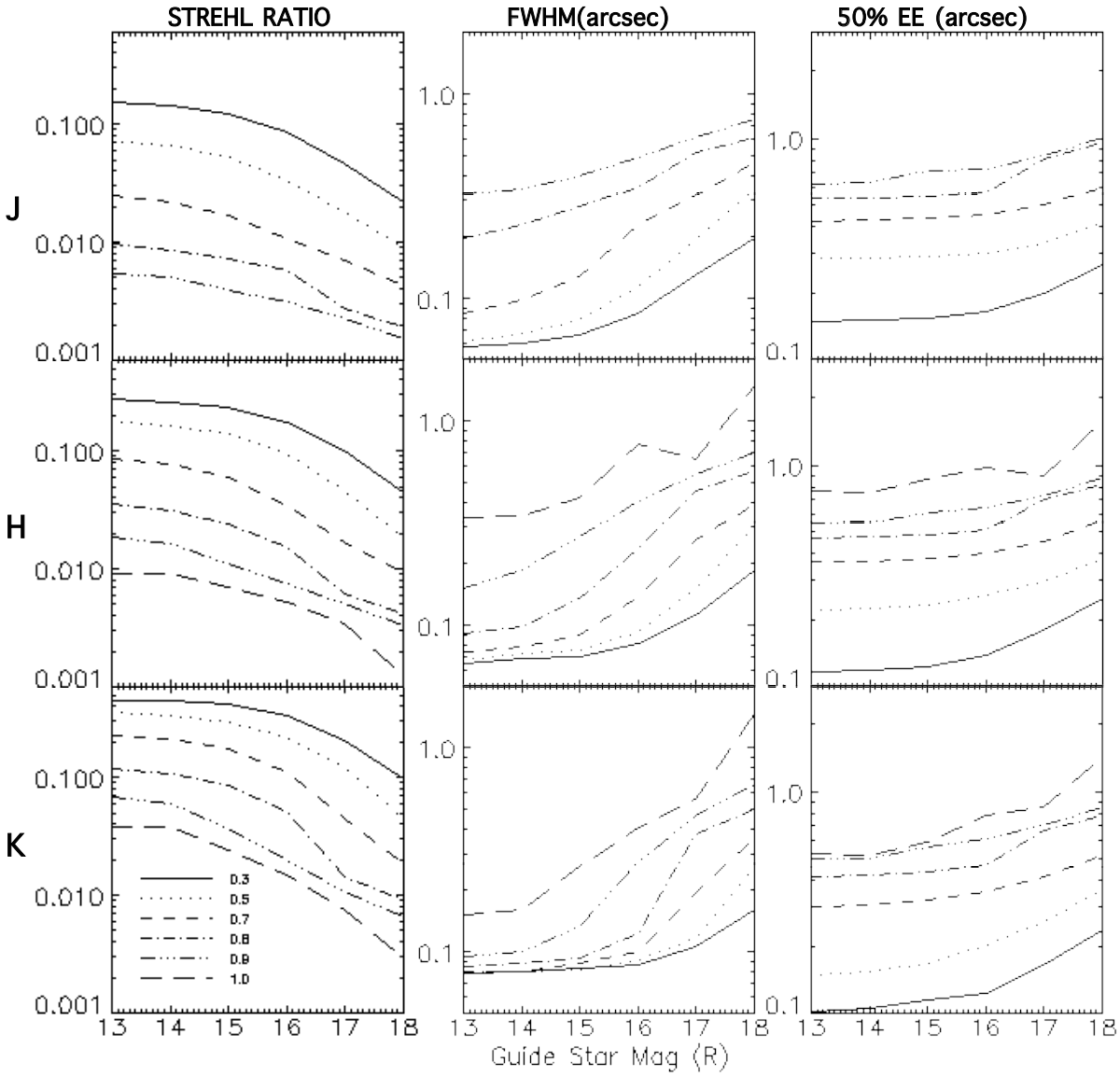

Figure 1. Degradation in AO performance (Hokupa'a curvature WFS) with guide star magnitude[3] with 0.3" to 1" seeing.

[3]http://www.gemini.edu/sciops/instruments/uhaos/uhaosPerfGSMag.html

I.5.3 - Natural Guide Star (NGS) Sky Coverage

AO correction requires a wavefront reference, usually a star in the field, of sufficient brightness for the system to lock and maintain positive adaptive control. Bright stellar targets (or extended targets with centrally-peaked or unresolved bright surface features) may serve as their own wavefront references. In general, a star of sufficient brightness must be found in the field of interest to be used as a natural guide star. Statistically, the fraction of the sky for which a guide star of a given R magnitude may be found, in a field of a given size, is illustrated in Figure 2 (delineated by galactic latitude).

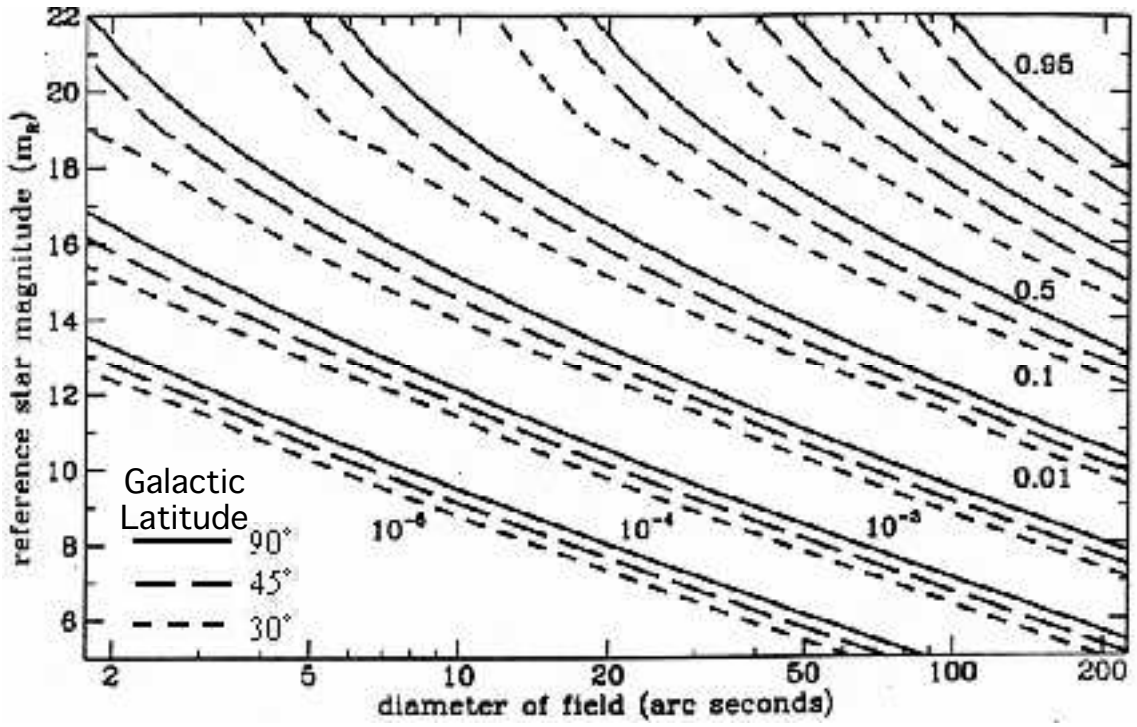

Figure 2. Sky coverage fraction (as a function of brightness and field size) of natural guide stars[4].

From this, one can estimate the all-sky integrated likelihood of finding a usable guide star for an AO system (e.g. see Table 3) within its isoplanatic angle (section I.5.1) and limiting guide star magnitude. For example, an AO system with an isoplantaic angle of 15" (30" field diameter) and an R = 14 guiding limit has access to ~ 1% of the sky. The situation is greatly improved for those systems with fainter guiding limits, with 30" field sky coverage approaching 10% at low galactic latitude (but less favorable for extragalactic, out-of-plane fields) for a limiting magnitude of R = 17.

[4]from: http://mthamilton.ucolick.org/techdocs/instruments/AO/index.html#AOsensitivity

However, at such faint guide star magnitudes the achievable Strehl ratio (and image quality) can suffer significantly (section I.5.2).

I.5.4 - Laser Guide Stars (LGS)

Artificial sodium or Raleigh "laser guide stars" hold promise to alleviate some of the limitations imposed by the natural distribution of astronomical sources used for wavefront references. LGS systems still require natural guide stars for tip/tilt (image centroid) corrections within ~ 30" of any particular target. Tip/tilt stars may be as faint as ~ R = 18, hence the total sky coverage, statistically, with an LGS system is ~ 50%, but may be as low as ~ 10% at high galactic latitudes (see figure 2).

Current LGS systems have been under test and limited uses for several years, but as of yet are still in early phases of development. The high-order Lick LGS/AO system can yield K-band Strehl ratios > 50% on nights with r_0 < 20 cm. Experiments with the AFLA LGS/AO system (a precursor to the VLT PARSEC system) on the similarly-sized (3.5-meter) Calar Alto telescope had reached an on-axis K-band Strehl ratio of 0.23 during a single "very best" 10s exposure with a 0.14" FWHM PSF during a series of "excellent nights"[5], indicative of the promise of LGS systems. Laser systems are being designed for larger telescopes, notably the sodium laser PARSEC system to be installed on the VLT/Yepun 8.2-meter telescope likely next year, and the LGS system to augment the Keck-AO facility which will likely be completed no sooner than 2004. Many operational details and system interface issues will have to be addressed before large telescope LGS systems are in routine use[6].

I.5.5 - Seeing

AO systems degrade with the atmospheric seeing conditions (whether natural or laser guide stars are used), and work at their peak performance only when the seeing conditions are matched to the design of an AO system at particular site. The wavelength dependent size of the seeing disk

---

[5]http://www.mpe.mpg.de/www_ir/ALFA/index.thml

[6]LGS systems may have externally imposed viewing constraints. For example, the Shane 3-m (Lick Observatory / Lowrence Livermore National Laboratory) AO+LGS system can only be used from midnight to 4AM and within 45° of the zenith due to FAA constraints, and target scheduling must be pre-approved by Space Command and is sometimes denied or permitted only restricted observing windows.

depends upon the atmospheric coherence length such that FWHM(λ) ~ λ / r_0 and is proportional to secant(β)$^{-3/5}$ $\lambda^{6/5}$. As an example, and AO system which can deliver an on-axis K-band Strehl for a star at the zenith under conditions of 0.3" seeing of 0.45 might typically yield a Strehl of 0.29 with 0.6" seeing, and 0.07 with 1" seeing. Commensurately, if the FWHM of the above star at the zenith was 0.08" and 50% energy encirclement at r = 0.1" with 0.3" seeing, it would degrade to a FWHM of 0.15" with 50% energy encirclement at r = 0.53" with 1" natural seeing.

I.5.6 - Zenith Distance (Airmass)

To first order the size of the instantaneous natural seeing disk (s) increases with zenith distance (z) as: s = secant(z)$^{3/5}$. Hence, all other variables being equal, AO correction is most effective when an object transits the meridian, and indeed the structure of the PSF and the achievable Strehl or EE for any given object varies with hour angle (i.e., with time). Moreover, the effectiveness of a given AO system is limited in target declination by the geographic latitude of the site. For example, at Mauna Kea (i.e., Keck, Gemini North, Subaru and CFHT at latitude +20°) potential targets in the recently discovered young and nearby star-forming associations in the southern hemisphere at declinations of -50° to -60° would have minimum airmasses of 3 to 6 and increased natural seeing disks of factors of 2 to 3, and thus would be better suited for a southern hemisphere facility (such as VLT).

I.6. – "TYPICAL" STREHLS - The Fallacy of Simplification

Because of the multi-dimensional and temporally variable phase space that ultimately determines the instantaneous Strehl, data to fully characterize these parametric dependencies of Strehls is often sparse (and for some systems unavailable). As a simplification, ground-based AO systems are typically characterized by "median" (or best) Strehls under idealized conditions, which (often) may not be realized in practice and must be viewed with caution. Results from a study using data from the AO system on the W.M. Keck II Observatory's 10-meter telescope[7], which illustrates this, are presented below.

The Keck AO system has 240 sub-apertures controlling a 349 actuator mirror. The control system is updated at a rate of 670 Hz with a bandwidth of ~ 25 Hz. The wavefront sensor is a silicon device with spectral sensitivity from ~ 0.4 to 1 μm. For this investigation, the system was used in closed-loop mode using natural guide stars of magnitudes $4 < V < 14$. (The Keck laser guide star system is still in development and has not been used with the AO system. It is unlikely that the Keck LGS system will be available for science observations until 2004 at the earliest). On-axis Strehl ratios were measured from a sample of 55 stars, serving as their own wavefront reference, over four years between 1998 and 2002 with target declinations $-60° < \delta < +65°$, probing a significant range of air masses. (The W.M. Keck observatory is at latitude of +20°).

Observations (filled triangles in Figure 3) were predominantly in H-band. Except for the ten stars measured in K-band, K-band performance was estimated from the H-band observations by scaling through the Marechal approximation. In this figure targets are broken into two declination zones: $\delta < -30°$ (> airmass ~ 1.7 at transit) and $-30° < \delta < +60°$. Specific air masses were not provided for individual observations, but most were taken near transit. Strehl ratios were measured for the AO corrected guide stars themselves (not other stars in the field, which may have been degraded due to anisoplanatism). Data were excluded for those cases where the AO system failed to lock onto the guide stars (which was estimated to be ~ 10% of the time when the seeing was "bad").

---

[7]These data have been kindly provided by B. MacIntosh, LLNL

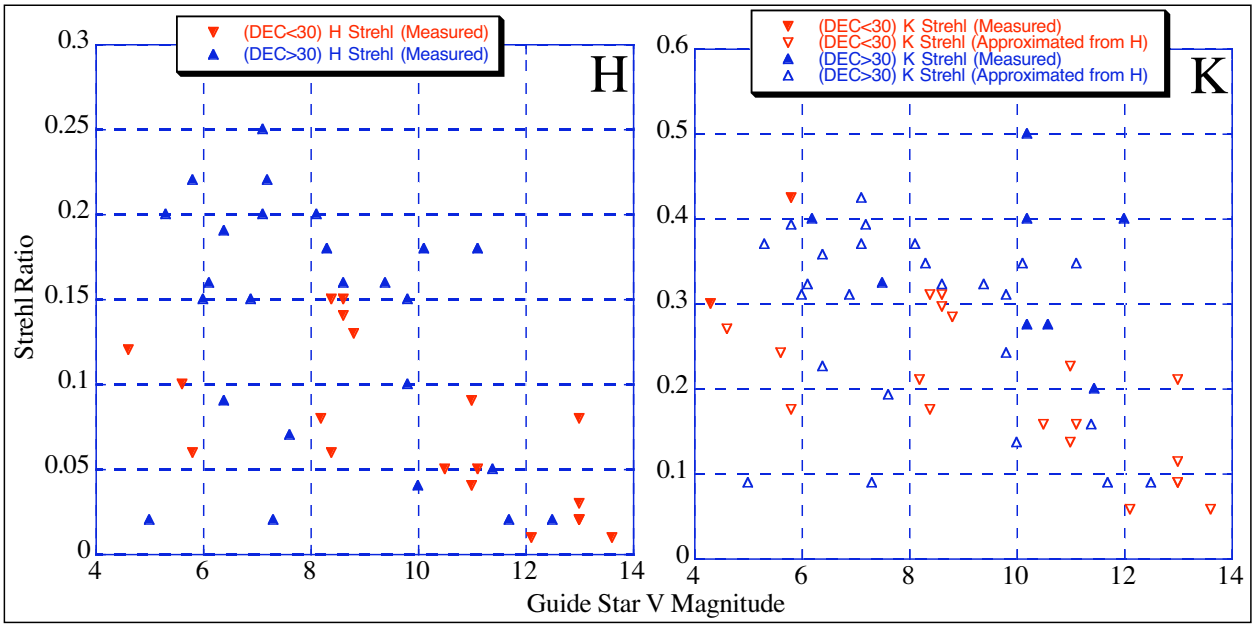

Figure 3. Strehl ratio vs. guide star V magnitude on Keck AO system.

Over the entire sample one obtains median Strehls of 0.10 in H and 0.23 in K, though there obviously is a strong dependence on guide star brightness (V) and declination (here used as a surrogate for airmass). Figure 4 illustrates the Strehl(V, δ) dependency, tiling any unsampled regions by 2D interpolation. In this figure the Strehls ratios achieved have been segregated into declination ranges ($-25° < \delta < +65°$; airmass at transit < 1.4) and ($-60° < \delta < -25°$; airmass at transit > 1.4) and in the guide star brightness ranges $4 < V < 9$ and $9 < V < 14$.

As expected brighter guide stars and lower air mass yield higher Strehls, though it is apparent that the dispersion about an expected "median" value is quite large. "Best" Strehls are obtained with bright guide stars, but statistically only about 1% of the sky has stars bright enough to provide a suitable wavefront correction within the isoplanatic AO correctable region (of ~ 10" from the guide star). Indeed, the effective V magnitude limit for AO enabled correction with the Keck system is at ~ magnitude 14. This situation is better for curvature sensors, which can lock and correct to fainter guide star magnitudes, but fall off significantly on the faint end. For example the Subaru AO system can provide ~ 2 – 18% Strehls at V=18 under conditions of exemplary seeing and low air mass. When spatial resolution, rather than image contrast, is the predominant driver for enabling a scientific goal, under some conditions such low Strehls (but significantly improved over natural seeing) can be sufficient. The air-mass degradation limits the range of sky which is effectively available from a given observatory site, and more stringently bounds the temporal observing windows for targets which do have suitable guide stars and transit high enough in the sky.

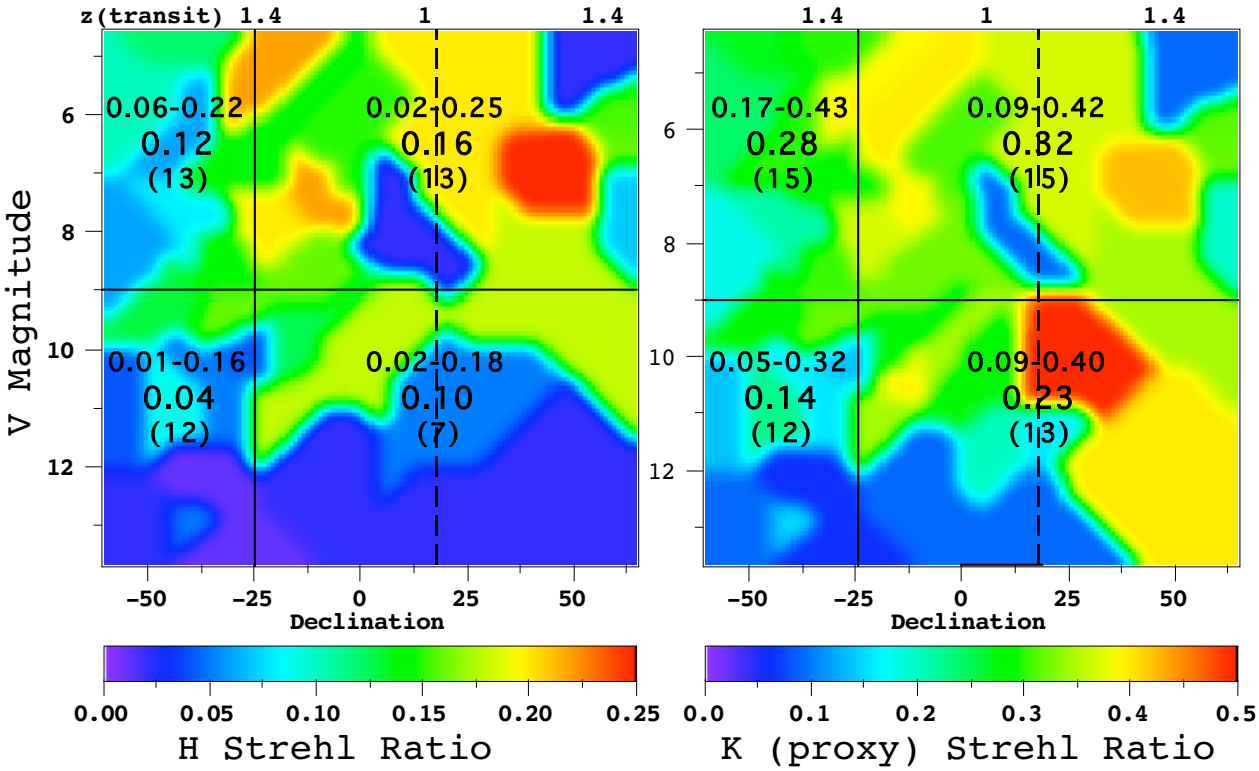

Figure 4. Strehl ratios with the Keck AO system (latitude = +20°) segregated by guide star brightness (at V=9) and declination (±45° from zenith at transit). Numbers in each sector indicate ranges of Strehls, median Strehl, and number of stars measured.

HST+NICMOS does not suffer from these limitations as its unyieldingly high Strehl is essentially invariant (and accessible) over the entire sky, and unreliant on the ground-based necessity of bright guide stars in close proximity. Laser guide star systems may pave the way for increasing the sky coverage for ground-based AO systems. Though those technologies are in development, they are far from routine in use at the few facilities where they are available and still are fickle and performance is strongly dependent upon sky conditions.

The Strehl ratios noted above from the Keck AO system apply for field-points in close angular proximity to the AO guide star, but fall off with distance as the atmospherically limited isoplanatic angle.

I.6.1 - AO System Descriptions and Performance Characteristics

Unbiased metrical comparisons between different, currently operating AO augmented telescopes (and with HST/NICMOS) are difficult because of the previously discussed caveats and variabilities that affect ground-based systems. Individual facilities characterize their AO system

performance in somewhat different terms, which are often non-homomorphic. Thus, trying to assess the degree of resource commitment (e.g. necessary observing time to achieve a quantifiable goal), and likelihood of success, of a specific observing program if attempted on such a facility requires careful, and critical, study and evaluation. Such evaluations cannot be captured in a simple summary, and readers are directed to up-to-date facilities/instrumentation descriptions as provided by the responsible and cognizant organizations themselves. A facilities list to URL's to on-line documentation (which tends to be more current than often more-dated information which appears in the literature) is provided in Table 2.

TABLE 2: On-Line AO system Documentation and Descriptions

CFHT/PUEO	http://www.cfht.hawaii.edu/Instruments/Imaging/AOB/description.html
VLT/NAOS	http://www.eso.org/instruments/naos/naos.html/
Gemini/Hokupa'a	http://www.us-gemini.noao.edu/sciops/instruments/uhaos/uhaosIndex.html
Keck II/AO	http://www2.keck.hawaii.edu:3636/realpublic/inst/ao/ao.html
Lick/AO NGS	http://mthamilton.ucolick.org/techdocs/instruments/AO/index.html
Lick/AO LGS	http://www.llnl.gov/urp/science/lgs_www/lgs.html
Palomar/PALAO	http://ao.jpl.nasa.gov/
Suburu/AO	http://subarutelescope.org/Observing/Instruments/AO/index.html
LaSilla/ADONIS	http://www.ls.eso.org/index.html
MSSS/AMOS	http://ulua.mhpcc.af.mil/
AFRL/SOR	http://wwwsor.plk.af.mil/sor/

To provide some basic information regarding a subset of these systems (which are discussed or noted elsewhere in this report) we have extracted and reproduced a few, hopefully representative, "as advertised" performance metrics. These summary data are not always presented on equal footing. Readers are strongly advised to consult the more complete user documentation provided by the individual facilities, and the performance levels suggested in this table are not assured under the different conditions of guide star brightness, seeing, wind speed, airmass, target declination, etc.

TABLE 3: Comparison of NICMOS and AO Systems

FACILITY	D	WFS	Strehl J%	Strehl H%	Strehl K%	FWHM(mas) J	FWHM(mas) H	FWHM(mas) K	IPA "	GS LIM	*	Instruments
HST/NICMOS	2.4	N/A	98	98	98	110	165	220	N/A	N/A	0	Cameras 1,2,3
CFHT/PUEO	3.6	CS+TT	27	41	56	95	110	140		14-17	1	KIR, OASIS, FOCAM
Keck II/AO	10	SH	15	35	50	35	40	50	~15	13-14	2	KCAM, NIRSPEC, NIRC2
Gemini/Hokupaa	8	CS	7	18	35	60	70	80	~10		3	QUIRC {NIRI}
LaSilla/ADONIS	3.6	SH+TT	3-9	5-20	9-40			150	~10	12	4	SHARPII, COMIC
Palomar/PALAO	5	SH	10		50	63		110		~12	5	PHARO
Lick/AO	3	SH	18	40	65			150	~20	12-13	6	IRCAL(PI inst)
Suburu/AO	8.2	CS	3	9	21	94	71	74	~40	17	7	CIAO, IRCS
VLT #4/NAOS	8	SH			70	40	52	69	~60	V18,K14	8	CONICA

* Notes:
D = Telescope diameter (meters), IPA = isoplanatic angle, GS = LIM guide star limit.
CS = Curvature Sensor, TT = Tip/Tilt, SH = Shack Hartmann Sensor

0. Strehl: (Camera 3) ~ 84-87%. FWHM: For F110W, F160W, F222M.No field dependence. No wavefront reference required.

1. With "median" seeing of 0.65" and "bright" GS. Reduce Strehl by 50% for J(GS)=14.5.
Rigaut et al 1998. Strehl ratios have been corrected for static aberrations of PUEO.
Actual images not compared to fully diffraction-limited images but to images obtained using the artificial point source with no turbulence.

2. Performance per Keck AO web site, but also see section 1.6.

3. For 0.5" natural seeing, target at zenith, on-axis, GS Mag R = 13.
H-band Strehl degradation: x0.7 when 10" off-axis from target (and by x0.4 at 20").
Hokupa'a is being replaced with ALTAIR, and QUIRC with NIRI. ALTAIR+NIRI is expected to deliver ~ 40% Strehl in H-band under median seeing conditions for bright GS.

4. Strehl(K)=30% for GS(V)=8. x2 Strehl(H) reduction 10" off-axis. Max recommended zenith distance = 50°.

5. 5m exposure, 10" GS distance.

6. Strehls for GS(V) = 10 and seeing (r0) = 15cm. LGS and NGS proposals on a shared-risk basis. Best performance late summer/early fall. For LGS tip-tilt star must be Rmag < 16. LGS restricted to midnight to 4AM and zenith distances < 45°.

7. Maximum zenith distance = 45°. For GS Rmag = 17 the system can still lock, but returns Strehl(K) ~ 3%.

8. *PREDICTED* performance with 0.65" (average) seeing @ Ks-band and GS Vmag=10 with spectral type A0V, "actual on-sky performance of NAOS might be different". IPA: Strehl degraded by ~ x3 for 60" off-axis target. GS LIM: Vmag > 16.5 is "on the border of feasibility" and closed-loop control is often not achieved.

Reference:

Rigaut, F., Salmon, D., Arsenault, R., Thomas, J.; Lai, O., Rouan, D., Véran, J. P. Gigan, P., Crampton, David, Fletcher, J. M., 1998, "Performance of the Canada-France-Hawaii Telescope Adaptive Optics Bonnette", PASP, **110**, 152

II - SCIENCE CASES AND CONSIDERATIONS

II.1 - Sky-Limited Observations: Background vs. Aperture

NICMOS offers significant sensitivity gains over ground-based telescopes at $\lambda < 1.8$ μm (shortward of the F160W (H-band) red cutoff) due to very low sky backgrounds at these wavelengths[8] (several hundred times smaller than from ground-based observatories). Future ground-based instruments with OH suppression, such as OSIRIS[9] (an integral field spectrograph in development for use with the Keck AO system) may prove competitive with NICMOS over narrow fields-of-view (< 10" x 10", compared to up to 52" x 52" for NICMOS) in H-band.

The high spatial resolutions achievable with large ground-based AO augmented telescopes (e.g. see section II.4) make their point-source sensitivities competitive with NICMOS at longer wavelengths (e.g. K band) where the thermal background from HST itself is significant. Hence, in this observational domain ground and space based observations complement each other. For example, the question of "which is better" for spatially resolved imaging of high redshift galaxies would depend on the galaxy morphologies and surface brightness distributions. NICMOS definitely will have better H-band sensitivity, and also possibly better K-band sensitivity for the diffuse and "fuzzy" parts of high-z galaxies, whereas ground-based AO telescopes may outperform NICMOS for the most compact features of the same objects. Additionally, for medium redshift galaxies ground-based AO augmented telescopes will be able to obtain spatially resolved spectroscopy, which cannot be done with NICMOS.

II.1.1 - Faint Galaxies

For studies of faint galaxies, HST/NICMOS offers some significant advantages over ground-based near-IR imaging with AO augmented telescopes. This is because HST/NICMOS has:

(a) about a 7 magnitude darker sky than can be obtained from the ground in the short wavelength (the J—H band) near-IR, effectively giving HST the sensitivity of a 60-meter ground-based telescope with detectors of similar quantum efficiency at these wavelengths.

---

[8]http://stsdas.stsci.edu/ETC/NIC/nic_img_etc.html
[9]http://www.astro.ucla.edu/~irlab/osiris/

(b) a sharp and repeatable PSF with nearly perfect Strehl and spatial high resolution (FWHM ~ 0.11"—0.16" in the J—H bands).

(c) a spatially and temporally invariant PSF over a large field of view (up to 52" x 52" per single image).

(d) very high dynamic range imaging, critical for studying the true nature of faint galaxies, since many exhibit large spatial variations in star formation rates, and a non-negligible subset have weak active galactic nuclei and/or nuclear starbursts. The non-destructive read-out modes of the NICMOS detectors and fast 16-bit A-to-D converters permit a sampling dynamic range of > 21 stellar magnitudes in a single 1000-second exposure.

Ground-based (including multi-conjugate) AO cannot deliver all of the above properties simultaneously, or individually with reliance and repeatability. The faint galaxy population at AB_{mag} = 24–28 has median sizes or half-light radii r_e = 0.2—0.3", with a steadily declining median size towards fainter fluxes (Odewahn et al 1996, Cohen et al 2002, Windhorst et al. 2003; Figure 5). Typical galaxy diameters, out to the faintest detectable surface brightness levels, are typically 5—6 times larger than the galaxy half-light radii. Hence, for reliable faint galaxies studies, images with both exquisite PSF and Strehl ratios as well as excellent surface brightness sensitivity need to be obtained over spatial scales > app. 1" across for every galaxy. Faint galaxy studies over wide fields are currently problematic from even the best ground-based sites. HST/NICMOS therefore is unique in this observational domain, since it spans the wavelength range 0.8—2.4μm with FWHM ~ 0.1"—0.2" over a > 50" x 50" field-of-view with a uniform PSF.

Even for nearby galaxies, high resolution HST/NICMOS imaging permits:

(a) better estimation of star formation rates through Paschen-α imaging (which cannot be done from the ground)

(b) tracing the stellar mass component; and

(c) extending the wavelength range to the longest possible color-lever at HST resolutions (in concert with HST's optical and UV imaging instruments) to study stellar populations.

Windhorst et al. (2002) have shown that at HST resolution ~20—25% of even nearby galaxy classifications change significantly, compared to the ground-based RC3 classifications, due to the lack of high spatial resolution over wide fields in ground-based images.

II.1.1.1 - A "Historical Note" of Significance

The spherical aberration in the HST primary mirror, uncorrected in WF/PC-1 images resulted in Strehl ratios of ~16%, which so severely compromised studies of faint galaxy morphology and their surface brightness distributions to yield almost nothing useful compared to the fully-corrected HST imaging instruments. This was true, even after applying deconvolution algorithms to the aberrated HST images[10]. These algorithms are by their very nature highly non-linear on faint extended objects, since a good fraction of the noise in the image arose from instrumental sources and field-dependent scattering (not diffraction) of light from the diffuse (and afocal) PSF halos, and hence could not be reliably deconvolved out. Consequently, the true nature of faint blue field galaxies became only obvious with the refurbished HST shortly after 1994, even though 1200 orbits of Medium Deep Survey time was spent on this with the aberrated telescope in 1990-1993. From experience of imaging 100,000's of galaxies with both HST WF/PC-1 and WFPC2, Strehl ratio's >>50% are essential for faint galaxy studies. Dynamic range here is the critically factor, or one does otherwise (literally!) not get the whole picture.

References:

Odewahn, S. C., Windhorst, R. A., Driver, S. P. & Keel, W. C. 1996, ApJ, **472**, L013

Windhorst, R. A., Taylor, V. A., Jansen, R. A., Odewahn, S. C., Chiarenza, C. A., Conselice, C. J, de Grijs, R., de Jong, R. S., MacKenty, J. W., Eskridge, P. B., Frogel, J. A., Gallagher III, J. S., Hibbard, J. E., Matthews, L. D., \& O'Connell, R. W. 2002, ApJ, **143**, S113

Windhorst, R. A., Cohen, S. H., Jansen, R. A., Odewahn, S. C., Driver, S., P., Kawata, D., Gibson, B. K., & Hopkins, A. 2002, in the Lowell Observatory Workshop on "The Outer Edges of Dwarf Irregular Galaxies", Eds. S. Oey & D. Hunter (E-published in http://www.lowell.edu/Workshops/Lowell02/posters.html)

[10] see: "The Restoration of HST Images and Spectra", 1990, STScI Workshop Proceedings, eds. R. L. White and R. J. Allen; and "The Restoration of HST Images and Spectra – II", 1993, STScI Workshop Proceedings, eds. R. J. Hanisch and R. L. White.

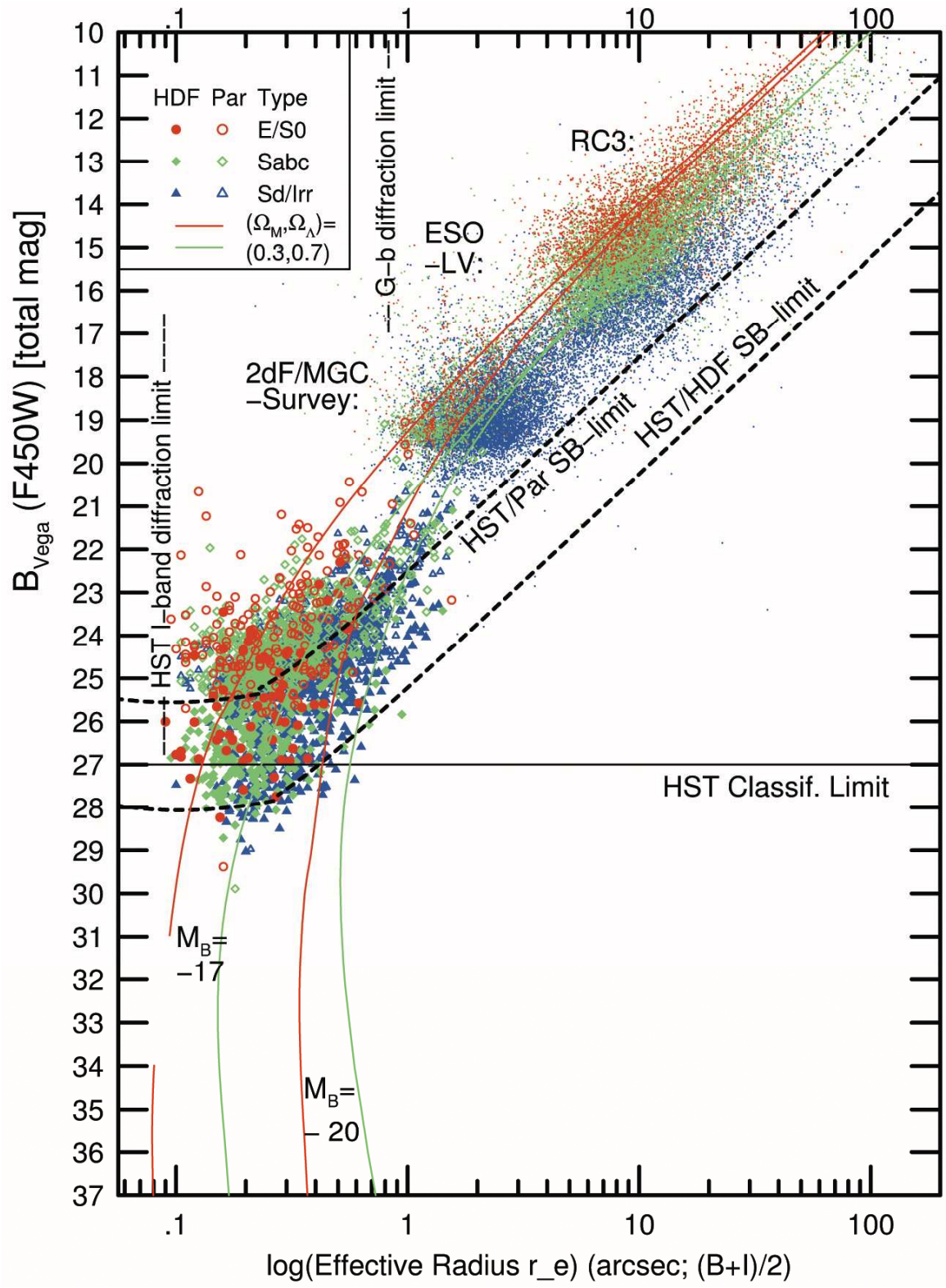

Figure 5. Distribution and detectability of faint galaxies as a function of half-light radius.

II.1.2 - Deep Imaging

The HST/NICMOS extremely low sky backgrounds (II.1.1(a)) shortward of K-band (where thermal emission from the telescope dominate) permit highly efficient and very deep high-resolution imaging of extragalactic targets (1I.1.1(b)) for cosmological studies, yet unmatched from the ground. This capability was demonstrated in HST cycle 7 with the NICMOS imaging of the Hubble Deep Field (GTO/7273; Thompson et al 1999), fully covering a 49.1" x 48.4" field in NICMOS camera 3 (Figure 6) previously imaged with WFPC-2 in the optical (Williams et al 1995) using 49 HST orbits in each of two passbands (F110W and F160W) in 7x7 position dithered grids. One hundred and forty seven 896s integrations were taken in each filter for total integration times of 36.5 hours. The final combined images resulted measured *1-sigma per pixel noise levels of AB magnitudes 31.7 and 31.9 in F110W and F160W* resulting in reliable detections of 342 galaxies (105 more than seen in the same WFPC-2 field) with *AB magnitudes as faint as ~ 30.0 in both bands*.

It should be noted that even at this depth *the images were not limited by sky background or instrumental systematics, and the noise reduction was still improving approximately as root(exptime)*, so additional integration time would have yielded fainter sources. Additionally, with the higher detector operating temperature of ~ 77K, NICMOS is now operating with significantly improved quantum efficiency as compared to cycle 7 (~ 60% at F110W and ~ 40% at F160W), and though the dark currents have been elevated to ~ 0.2—0.3 electrons/second, such exposure depths (and beyond) can now be reached with even greater efficiency.

References:

Thompson, R.I., Storrie-Lombardi, L.J., Weymann, R.J., Rieke, M.J., Schneider, G., Stobie, E., and Lytle, D., 1999, "NICMOS Observations of the Hubble Deep Field: Observations, Data Reduction, and Galaxy Photometry", Astronomical Journal, **117**, 17

Williams, R. E., Blacker, N., Dickinson, M., Dixon, W. V. D., Ferguson, H. C., Fruchter, A. S., Giavalisco, M., Gilliland, R. L., Heyer, I., Katsanis, R., Levay, Z., Lucas, R. A., McElroy, D. B., Petro, L., Postman, M., Adorf, H-M, Hook, R., 1996, "The Hubble Deep Field: Observations, Data Reduction, and Galaxy Photometry", Astronomical Journal, **112**, 1335

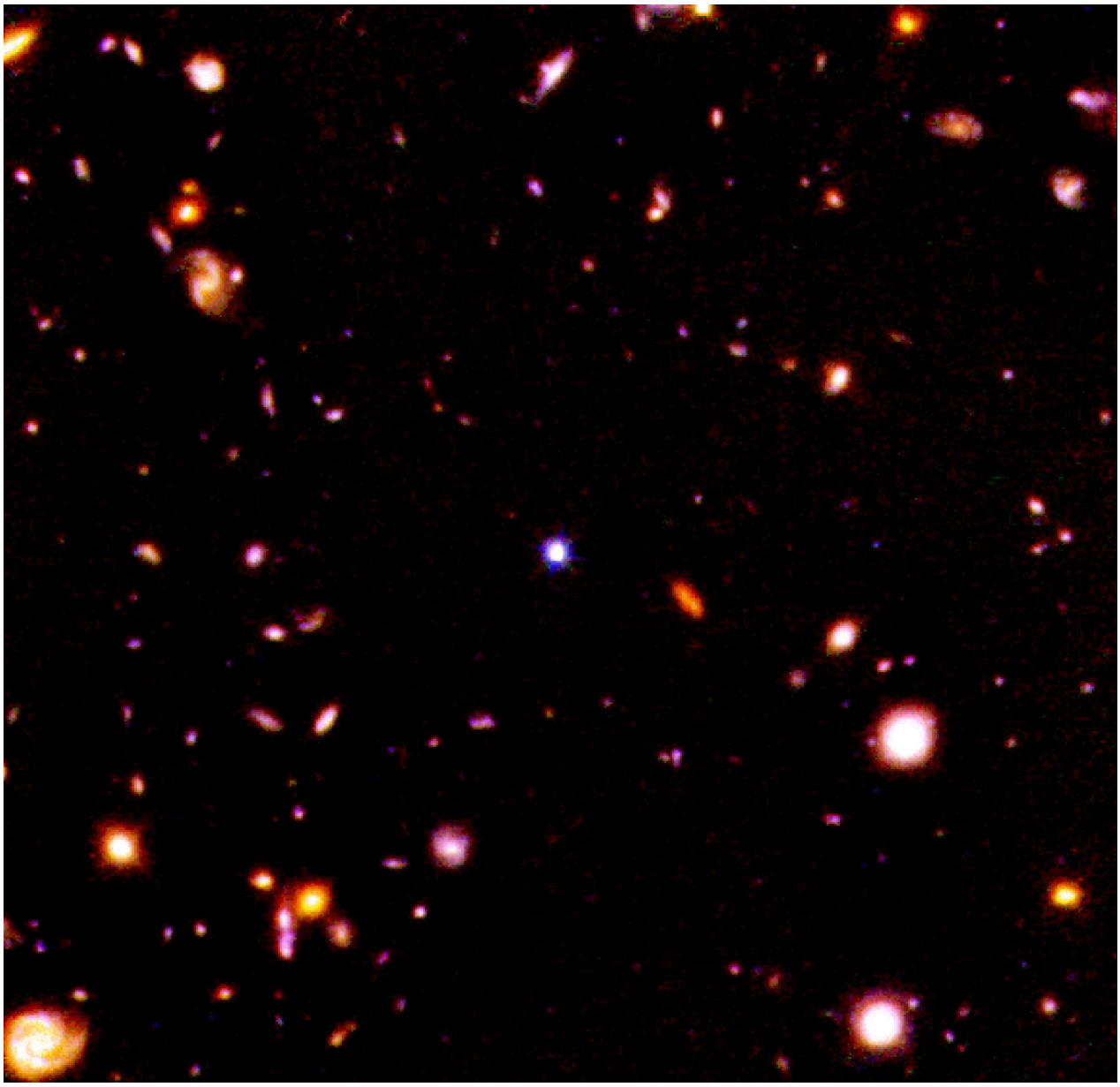

Figure 6. The NICMOS Hubble Deep Field from GTO/7273.

II.2 - Crowded Field Photometry/Astrometry

HST+NICMOS compares very favorably to ground-based AO and speckle techniques in crowded, confusion-limited, regions such as the galactic center and in stellar clusters in terms of source detection, photometric precision, and astrometric accuracy due to the intrinsic stability of the PSF coupled with its high and spatially invariant Strehl ratio. We illustrate two published science results where field crowding sets the limiting systematics for the scientific goals.

II.2.1 - The Arches Cluster

The mass-function of the Arches cluster (30 pc from the galactic center) was studied by two groups using ground-based adaptive optics and HST/NICMOS imaging. Stoltie et al (2002) used the GEMINI/Hokupa'a curvature sensing AO system (Graves et al 2000), which "typically" delivers Strehl ratios between 5% and 25% in K-band. H-band (FWHM = 0.19") and K'-band (FWHM = 0.135") images were obtained with the QUIRC near-IR camera (Hodapp et al 1996) equipped with a HgCdTe array yielding a 20.2" field-of-view with with 0.02" pixels. Data were acquired over a period of one month with total H and K band integration times of 720s and 1040s, respectively, combined from dithered 60s and 30s exposures taken under conditions of "excellent seeing".

Figer et al (2002) imaged the Arches cluster with HST/NICMOS in GO program 7364 on 14 September 1997. The NICMOS images were obtained with much shorter total integration times of 256s (36% and 25% as long as the Gemini images in the equivalent passbands) with the intermediate resolution camera (2), but critically sampled the PSF with 0.076" pixels. The HST/NICMOS images were taken in F160W and F205W filters (commensurate with the Gemini H and K' filters), yielding stellar images with FWHMs of 0.16" and 0.20", respectively, and hence roughly comparable to the reported Gemini/Hokupa'a spatial resolutions.

The Gemini images were photometrically calibrated using the HST/NICMOS images to transform instrumental counts into in-band absolute magnitudes. Figure 7, reproduced with highlighted annotation from Stoltie et al (2000), shows the observed radial variation in the stellar luminosity function with distance from the cluster center (which becomes confusion limited near the cluster core). Observed star counts for NICMOS F205W are dashed lines, and GEMINI K' are the solid lines. (The dotted lines are derived from the Gemini data after applying an incompleteness correction). In each radial zone the star counts roughly agree for the brightest stars, but diverge

significantly for fainter members which were undetected in the GEMINI data (regions in red) despite the longer integration times and reported roughly comparable PSF FWHM.

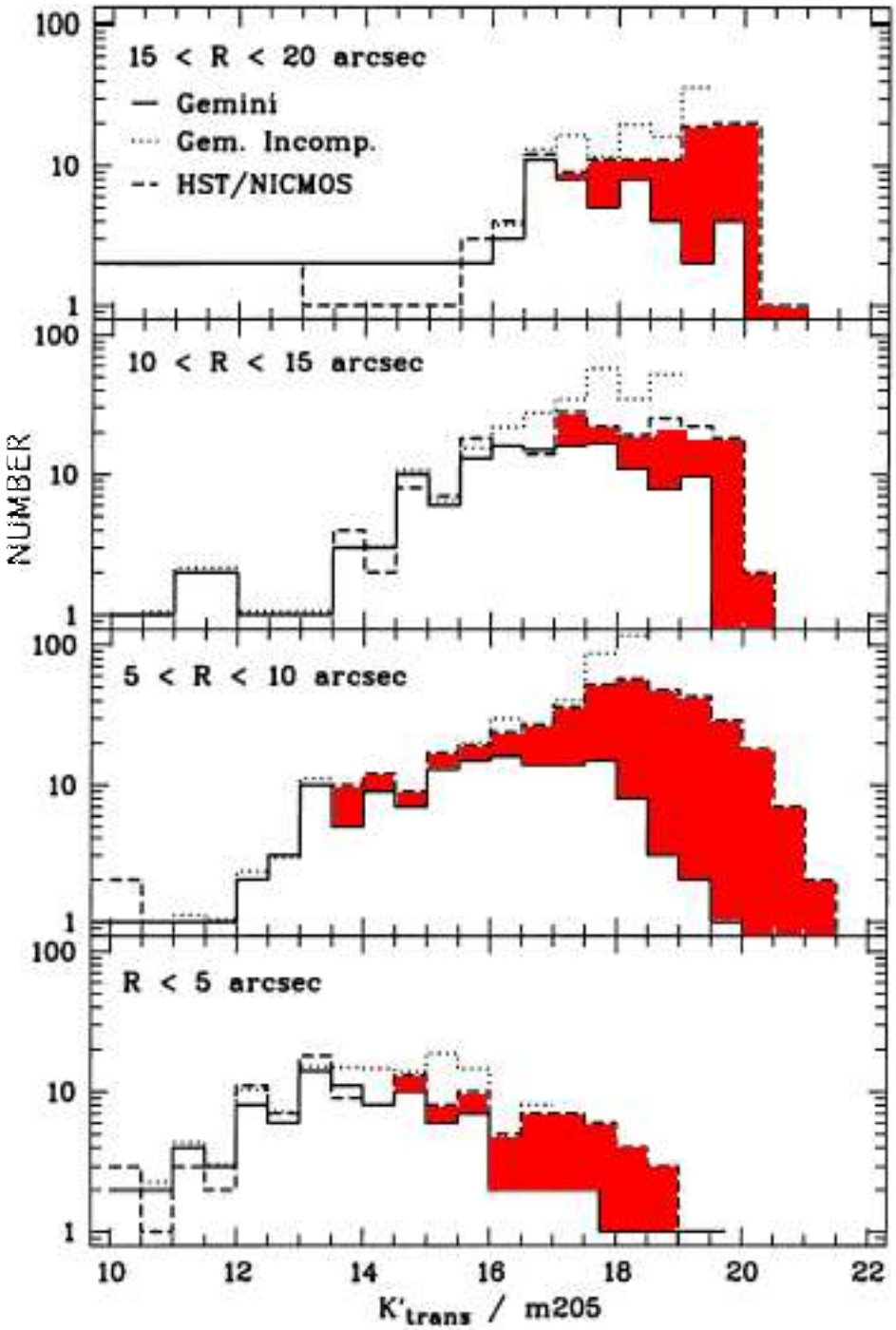

Figure 7. NICMOS and Gemini/Hokupa'a recovered star counts in 5" wide annular zones centered on the Arches cluster (from Stoltie et al 2000). The red regions represent stars extracted from the NICMOS data but not imaged in the Gemini/Hokupa'a image.

The derived de-reddened slope of the mass function, as determined from the Gemini and NICMOS data sets (Figure 8) agree within their formal errors, but only to a lower limit of ~ 13 solar masses. But, because of the inability of the Gemini/Hokupa'a observations to recover stars as faint as seen in the NICMOS images in this crowded field, the Gemini data would imply a turn-over in the mass function for less massive stars due to sample incompleteness. However, the NICMOS camera 2 data effectively probe the mass function to a lower limit of ~ 2 solar masses, a factor of approximately 6.5, in mass, deeper than the Gemini/Hokupa'a data.

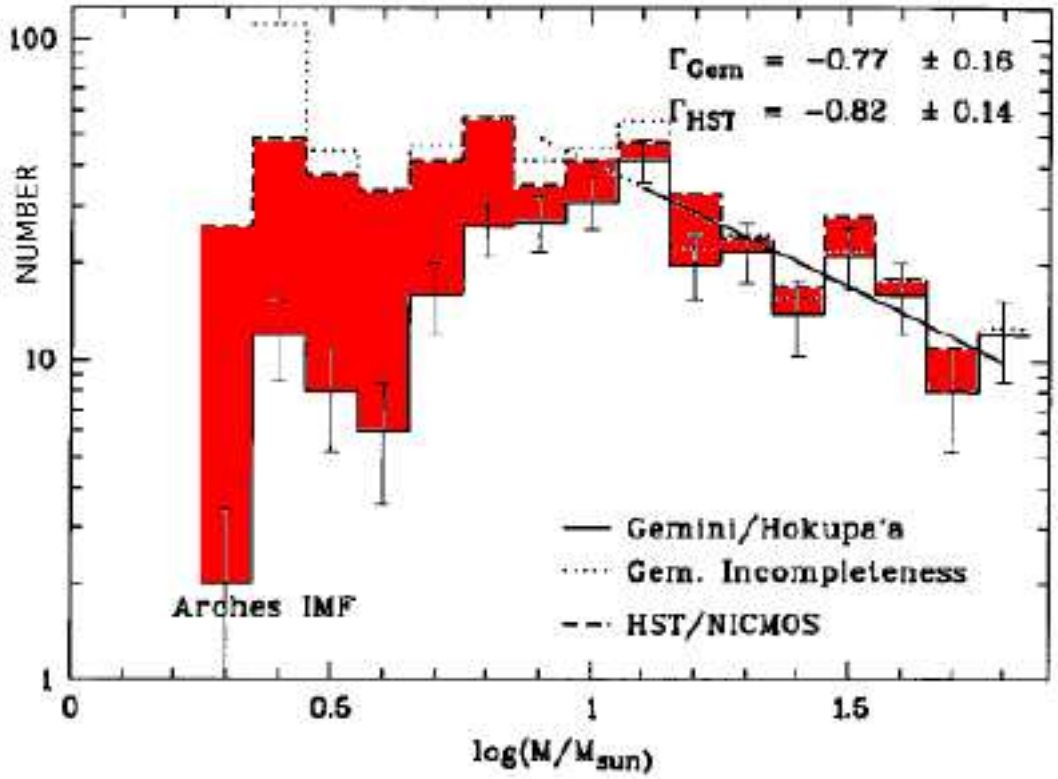

Figure 8. Stellar mass functions for the Arches cluster as measured from the NICMOS and Gemini/Hokupa'a images (Stoltie et al 2002).

This cluster and the Quintuplet cluster, also ~ 30 pc from the galactic center and studied with NICMOS by Figer 1999, appear to have flatter IMFs richer in high mass stars than is typical for the solar neighborhood and may be indicative of what is seen in starburst galaxies.

References:

Figer, D. F., Kim, S. S., Morris, M., Serabyn, E., Rich, R. M., & McLean, I. S., 1999, "Hubble Space Telescope/NICMOS Observations of Massive Stellar Clusters near the Galactic Center", ApJ, **525**, 750

Figer, D. F., Najarro, F., Gilmore, D., Morris, M., Kim, Sungsoo, S., Serabyn, E., McLean, I. S., Gilbert, A. M.; Graham, J.R., Larkin, J. E., Levenson, N. A. & Teplitz, H. I., 2002, "Massive Stars in the Arches Cluster", ApJ, **581**, 258

Graved, J. E., Northcott, M. J, Roddier, F. J., et al 2002, SPIE, **4007**, 126

Hodapp, K. W., Hora, J. L., Hall, D. N. B., et al 1996, New Astron., **1**, 177

Stolte, A. Grebel, E. K., Brandner, W., & Figer, D. F., 2002, "The Mass Function of the Arches Cluster from Gemini Adaptive Optics Data," A&A, **394**, 459

II.2.2 - The Galactic Center

The galactic center, heavily obscured in the optical, is only moderately extincted at near-IR wavelengths, and the crowded field is confusion limited from multiple, overlapping sources. NICMOS observations of the galactic center were obtained by Rieke (1998) to investigate possible stellar variability and study the dynamics, star formation history, and IMF in the immediate vicinity of the central ~ 2.5×10^6 solar mass black hole candidate SgrA*. Even in this very crowded field, the highly stable HST+NICMOS PSF enabled highly accurate multi-color photometry and searches for stellar variability on timescales of minutes to months (Figure 9). Temporal variability of tens of minutes is diagnostic of the scale of accretion disks, days for stellar winds, and months for microlensing. The nearly invariant PSF and high spatial resolution allowed setting an upper limit to the 1.6 μm dereddened flux from SgrA* of 18mJy, constraining advection dominated accretion flow models of the central black hole.

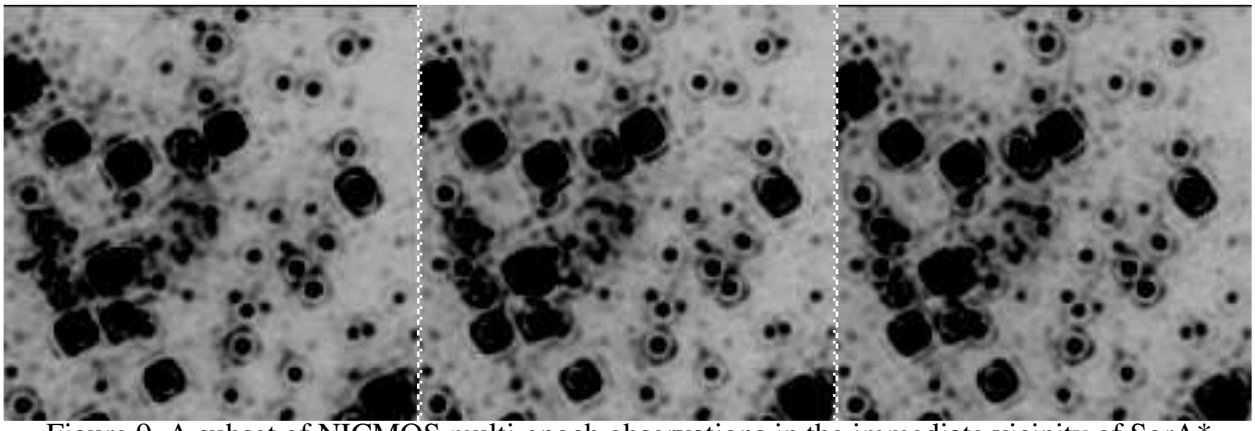

Figure 9. A subset of NICMOS multi-epoch observations in the immediate vicinity of SgrA* region of the galactic center spanning 8 months illustrating the stability of the PSF.

NICMOS provides diagnostic filters for high spatial resolution emission line imaging, notably ground-inaccessible Pα at 1.875 μm (~ 30 times stronger than Br γ at 2.166 μm, which is observable from the ground) which, by analogy to starburst galaxies, can reveal newly formed stars and shocks (Figures 10 and 11; Rieke 1998).

We compare NICMOS broadband and ground-based imagery of the galactic center first with speckle imaging reported by Genzel et al 2000, and then with recent AO imaging discussed by Schodel et al. 2002. Genzel et al used the MPE-SHARP camera (Hofmann et al 1993) employing a NICMOS-3 detector on the ESO 3.5-meter New Technology Telescope, with 0.025" and 0.050" pixels to oversample the ~ 0.15" FWHM diffraction-limited NTT K-band PSF. Data were acquired at nine epochs spanning five years with very short integrations of ~ 0.4s on nights of "very good

seeing" and several thousand frames at each epoch were coadded with the simple-shift-and-add (SSA) algorithm (Christou 1991; Eckart et al. 1994). It was estimated that the diffraction-limited cores of the resulting SSA images contained ~ 20% of the total stellar light.

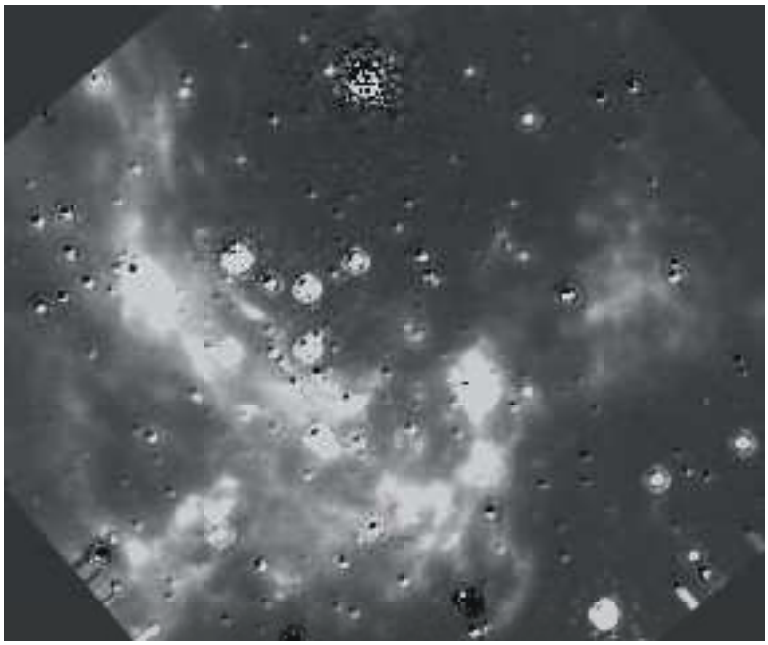

Fig 10. NICMOS Pα imaging of the galactic center. No emission is clearly associated with SgrA*, but highly structured emission is apparent with blue post-MS stars indicative of dense circumstellar shells. Bullets and tails from late-type stars are seen as a cavity around a B0 supergiant.

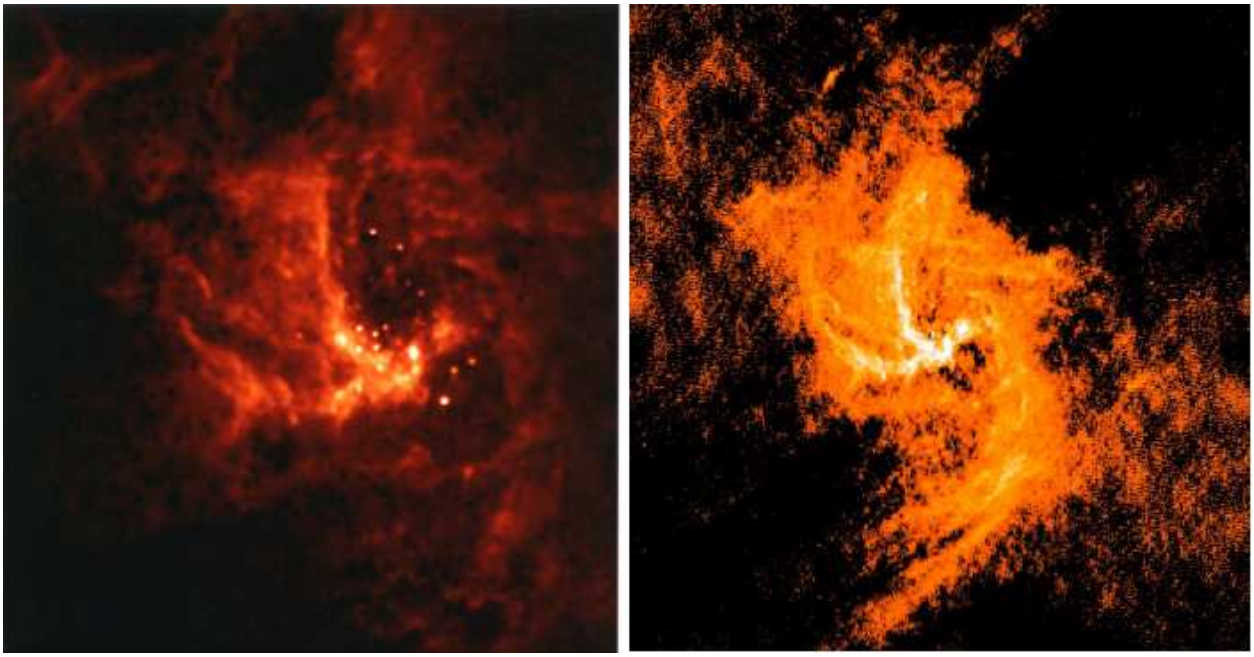

Fig 11. Larger scale NICMOS Pa (left) and VLA 2cm (right) imaging of the galactic center. VLA observations are unaffected by extinction but cannot detect high density regions.

The NICMOS image in Figure 12 (left) is portion of a median combination of four 24s H-band (0.16" FWHM) dithered images in the region of SgrA* obtained over a small fraction of an HST orbit (in which other filters were used to obtain multi-spectral images), yielding an effective integration time of 96s. The 147 red dots in overlaid on the image indicate the positions of stars detected in the NICMOS image but not in listed in the Genzel et al 2000 compendium listing of "all" 62 stars in the central 4 arcsecond region of the galactic center, found in their data set.

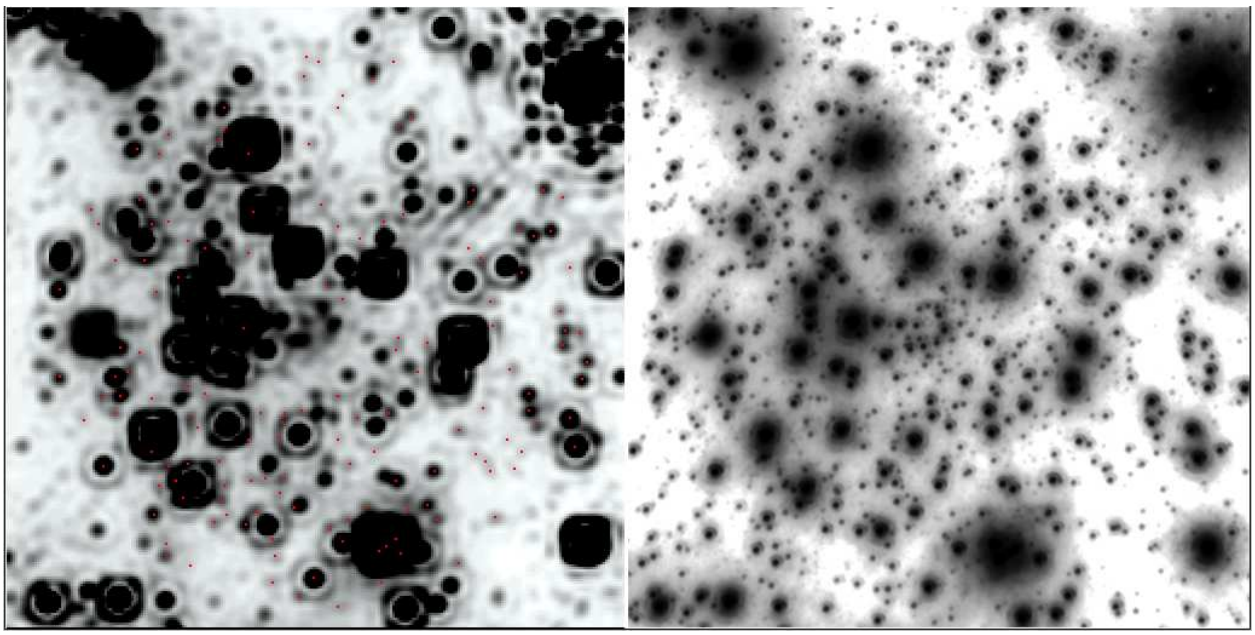

Figure 12. Left: NICMOS F160W (1.6 μm, H-band) image of the galactic center within ~ 5" of SgrA*. Red dots indicate stars undetected by Genzel at al with speckle imaging at the NTT. Right: Ks-band (2.1μm) image with the VLT CONICA/NAOS AO system[11]. The field is less obscured by extinction at Ks than H, and more stars are seem in the longer wavelength image.

More recently, Schoedel et al 2002 used the CONICA/NAOS imager on the 8 m UT4 telescope of the VLT and obtained diffraction limited (FWHM = 60 mas) Ks-band images of the galactic center (Figure 12, right) under conditions yielding ~ 50%Strehl. CONICA/NAOS is currently unique in having a near-IR wavefront sensor, which was used to close the AO loop in this optically obscured region using the bright supergiant IRS 7 only 6" from SgrA*. The resulting image is astrometrically competitive with, and perhaps superior to the NICMOS image for determining differential stellar positions, and lead to an improvement the position of SgrA* radio source with respect to the galactic center stars by a factor of ~ 3 (now with a 1 σ uncertainty of ±10 mas) over previous ground-based results. These positional astrometric results demonstrate the benefits that can be had from the smaller PSF FWHM that can be obtained with AO augmentation

[11]Courtesy of Reinhard Genzel, Max-Planck-Institut fur extraterrestrische Physik

on an 8-10 meter class telescope. Combined with (AO augmented) spectroscopy of the region, which cannot be done with NICMOS, radial velocities of the galactic center stars in conjunction with proper motions (from multi-epoch observations) can tightly constrain the orbits of the galactic center stars, and the mass of the central black hole.

References:

Christou J. C., 1991, Experimental Astron., **2**, 27

Eckart A., Genzel R., Hofmann R., Sams B. J., Tacconi-Garman L. E., Cruzalebes P., 1994, in Genzel R., Harris A. I., eds, The Nuclei of Normal Galaxies. NATO ASI Kluwer, Dordrecht, p. 305

Genzel, R., Pichon, C., Eckart, A., Gerhard, O. E. & Ott, T., 2000, "Stellar dynamics in the Galactic Centre: proper motions and anisotropy", MNRAS, **317**, 348

Hofmann R., Blietz M., Duhoux P., Eckart A., Krabbe A. & Rotaciuc V., 1993, M. Ulrich, ed., Progress in Telescope and Instrumentation Technologies. ESO Report **42**, 617

Rieke, M., 1998, "NICMOS Observes the Galactic Center" in NICMOS and the VLT: A New Era of High Resolution Near Infrared Imaging and Spectroscopy, Pula, Sardinia, Italy, June 26-27th 1998 ESO Conference and Workshop Proceedings, **55**, Wolfram Freudling and Richard Hook eds., 133

Schodel, R., and 22 co-authors, 2002, "Closest Star Seen Orbiting the Supernassive Black Hole at the Centre of the Milky Way", Nature **419**, 694

II.3 - CORONAGRAPHY OF CIRCUMSTELLAR ENVIRONMENTS

HST provides an unparalleled venue for high contrast imaging that has enabled new observational domains in exo-planet and debris disk imaging. Imaging dust and debris that might agglomerate to form planets around young stars has been technologically challenging because of the very high star-to-disk contrast ratios. Such contrast-challenged observations are extremely difficult from ground-based platforms, even with AO augmented systems, because of residual uncompensated effects of atmospheric turbidity. The resulting temporal instabilities in ground-based point spread functions set systemic detectability limits which are often under-appreciated, and overlooked, when instrumental performance is expressed with presumptively static metrics such as Strehl ratios (Schneider and Silverstone 2002). These limitations are greatly relaxed with HST. Unburdened by atmospheric seeing, NICMOS repeatably achieve very low levels of background contamination from the wings of stellar point spread functions (PSF). The stability of the platform allows scattered and diffracted light to be further reduced by two additional orders of magnitude through subtraction of the spatially and temporally highly-stable PSF and permits the removal of mid and high spatial frequency optical artifacts to a degree unchallenged from the ground (Schneider and Stobie 2001). The non-destructive read-out modes of the NICMOS detectors permit sampling the PSF, with its strong radial brightness gradient, over a dynamic range exceeding 5×10^7 in a single spacecraft orbit. Coronagraphy (in NICMOS camera 2) provides additional contrast gains approaching an order of magnitude at small angular distances from occulted stars, and in wavelength regimes where young (<~ 10Myr) Jovian-mass exoplanets are strongly self-luminous and thus may be imaged directly (Schneider 2002a).

NICMOS PSF-subtracted coronagraphy routinely results in per-pixel H-band background rejections of ~ 10^7 of an occulted target's total flux density at an angular distance of 1" (Figure 13), thus providing a high contrast lever for direct detection of close sub-stellar companions. At 1.1 μm, with a spatial resolution of ~ 0.1", occulted starlight is reduced by a factor of 10^5 integrated over a 2"–3" annulus, thereby enabling the direct detection of low surface brightness material in circumstellar environments, and as close in as 0.3" (at the edge of the coronagraphic mask) for disk with large scattering fractions (Schneider 2002b). We discuss both of these challenging observational domains of critical importance in furthering our understanding of the formation, evolution, dynamics and constituent properties of exo-solar planetary systems, their environments.

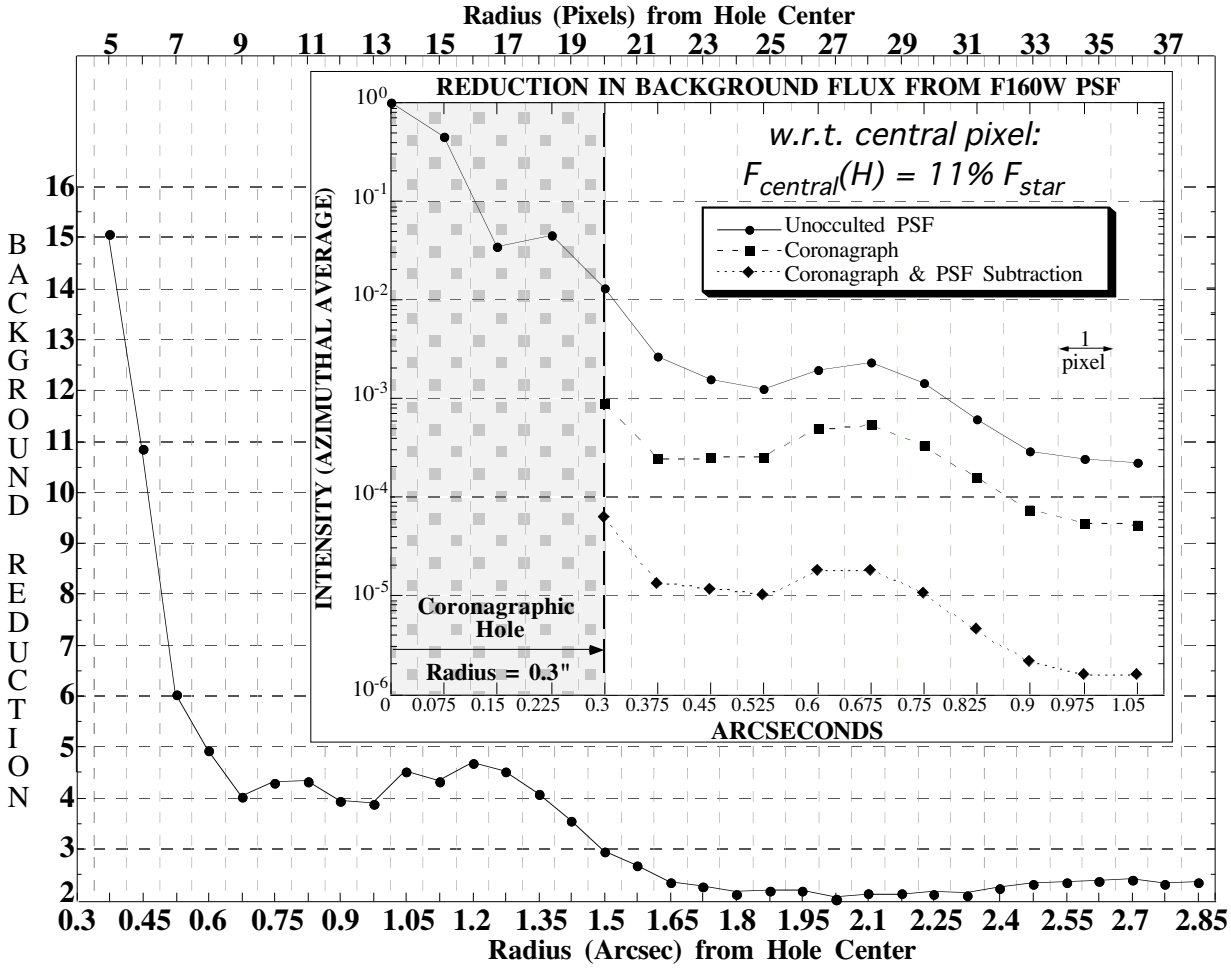

Figure 13. NICMOS H-band coronagraphic per-pixel background rejection (@ $r < 3$") and relative intensity with, and without, PSF-subtraction (@ $r < 1$") compared to unocculted central pixel (divide by 9 to compare to total starlight). From Schneider 2002c.

References:

Schneider, G., & Stobie, E., 2001, "Pushing the Envelope: Unleashing the Potential of High Contrast Imaging with HST", Conference Proceedings: ADASS XI, (ASP Conference Series), in press.

Schneider, G., 2002a, "High Contrast Imaging and the Disk/Planet Connection" Conference Proceesings: Hubble's Science Legacy: Future Optical-UV Astronomy From Space", ed. C. Blades, (ASP Conf Series), in press.

Schneider, G., 2002b, "Coronagraphy with NICMOS", Conference Proceedings: The 2002 HST CalibrationWorlshop, S. Arribas, A. Koekemoer, and B. Whitmore, submitted.

Schneider, G., and Silverstone, M., 2002, "Coronagraphy with HST/NICMOS: detectability is a sensitive issue", Conference Proceedings: High-Contrast Imaging for Exo-Planet Detection, SPIE Conf. Ser., in press.

Schneider, G., 2002c, "Coronagraphy with NICMOS", Conference Proceedings: The 2002 HST CalibrationWorlshop, S. Arribas, A. Koekemoer, and B. Whitmore, submitted.

II.3.1 - Debris Disk Imaging

Proto and young (<~ 10 Myr) circumstellar disks, with embedded or centrally obscured central stars, may be imaged directly with HST. Older debris and transitional disks, centrally cleared (e.g. by Poynting-Robertson drag and radiation pressure) present a contrast challenge readily addressed by NICMOS PSF-subtracted coronagraphy. Until NICMOS, the only debris system imaged in scattered light was the very large and edge-on disk round β Pictoris (Smith & Terille, 1985), while in its first six months of operation the modest (22 target) NICMOS/GTO disk survey added HR 4796A (Schneider et al 1999), HD 141569A (Weinberger et al 1999), and TW Hya (Weinberger et al 2002) of similar ages but smaller physical and angular extents.

The central stars of such disk systems are very bright (in these specific cases V = 5.7, 7.0, and 11.1, and for ground-based AO systems serve as their own wave-front references. The disks themselves are also very bright with high surface brightnesses due to their large scattering fractions (in these cases the fractional excesses due to the disks on the order of 0.1% that of the stars). These disks are angularly much smaller than the isoplanatic regions of AO systems (the largest, HD 141569A being only 4" in radius on the projected major axis). Brightness is not a critical detectability issue for disks such as these (so the light-gathering power of 8-10 meter class telescopes is not necessary) and relatively short exposure times would be sufficient in the absence of other systematics.

If well placed in the sky (at relatively low-airmass at transit) stars such as these should yield, under good natural seeing, a “high” Strehl ratio as characterized for a given AO system. Imaging such disks from the ground, however, has proven extremely challenging even with the advent of AO augmented technologies and only a few confirmable results have thus-far appeared in the refereed literature - most being follow-ons to HST observations. We consider recent ground-based follow-up observations to the three disk systems noted above, which are sensitivity and detectability limited by the stability and reproducibility of the instrumental PSF.

II.3.1.1 - HD 141569A (Herbig Ae/Be Star, ~ 5 Myr)

The difficulties involved in ground-based imaging of debris disk are illustrated by a recent successful observation of the HD 141569A circumstellar disk, first imaged in a single spacecraft orbit by NICMOS in 1998 (Weinberger et al 1999). Boccaletti et al (2003) observed HD 141569A over two nights, May 9 & 10 2001, using the PALAO 241-actuator adaptive-optics system on the

Palomar 5-meter telescope and IR camera (Haywood et al 2001) with coronagraphic imaging. The PALAO K-band observation, with comparable angular resolution to the NICMOS 1.1 μm image (both 0.11"), revealed the disk for the first time with a ground-based near-IR imaging system . Total integration times on target (and similarly bright PSF reference stars) were similar for the NICMOS and PALAO disk observations (shown in Figure 14) being 1216s and 1040s, respectively.

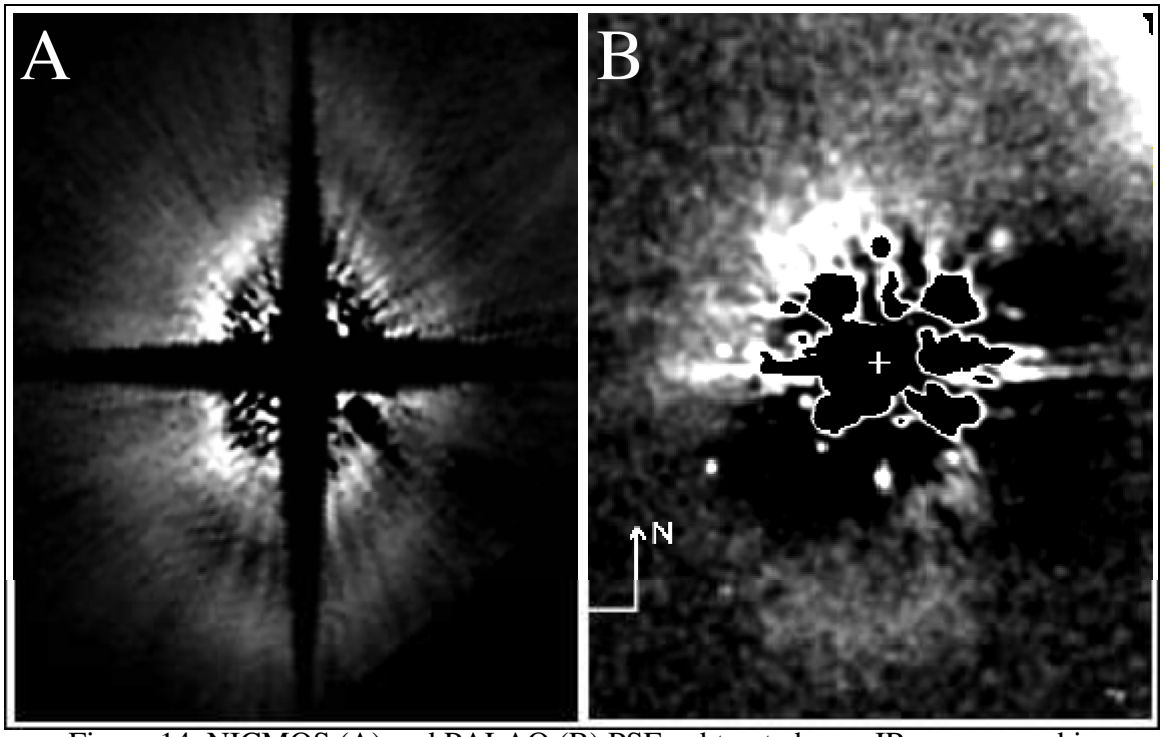

Figure 14. NICMOS (A) and PALAO (B) PSF-subtracted near-IR coronagraphic observations of the HD 141569A circumstellar disk.

This observation demonstrates the feasibility of detecting moderately sized (> few arcsecond) and moderately bright debris disks with high-order adaptive optics systems on large telescopes (at low air mass), and is a significant achievement given the image contrast of the disk in its close proximity to HD 141569A. However, the difference in image quality (and spatially resolved structure) is readily apparent, though the two instrumental systems had nearly identical spatial resolutions. The HD 141569A disk was not very contrast-challenging for NICMOS, as the surface brightness of the "inner ring" was ~ 270 μJy arcsec^{-2}, and the "outer ring" (1.7 times further from the star) about two times fainter (compared to the ~ 3.1 Jy F110W flux density of HD 141569A itself). Regarding the PALAO observations Boccatelli et al note: "it is still difficult to disentangle between circumstellar material since diffraction residuals are dominating the signal close to the mask. {Because the subtraction process is not perfect the stellar diffracted light dominates at close angular distance (r < 1.5")}. However, it was possible to unambiguously

identify the circumstellar component by comparing our image with the ones obtained using the HST."

Also according to Boccatelli et al. 2003: "the system {PALAO} can reach an average Strehl ratio of about 50% for bright stars (V < 7) under 1" seeing at near-IR wavelengths, and Strehl ratio as high as 68% have occasionally been obtained with very good seeing". However, the data obtained on 10 May 2001 were unusable due to "poor AO performance and mask centering". They estimate the actual Strehl ratio achieved for the May 9 observations was 16%, though HD 141569A transits at very low (favorable) airmass of 1.1 from the Palomar Observatory.

We note, that at this age and distance (5 Myr @ 100 pc) a gas-giant companion with a mass in the range of 2–3 Jupiters would have detectable (if one were to exist) in the partially-filled "gap" between the inner and outer rings resolved in this NICMOS image, an added benefit of observing in the near-IR with high spatial resolution and stary-light rejection.

References:
Boccaletti, A., Augereau, J. C., Marchis, F., Hahn, J., 2003, "round-based near-infrared imaging of the HD141569 circumstellar disk" ApJ, in press. (to appear March 2003); astroph: astro-ph/0211648
Weinberger, A. J., Becklin, E. E., Schneider, G., Smith, B. A., Lowrance, P. J., Silverstone, M. D., and Zuckerman, B., 1999, "The Circumstellar Disk of HD 141569 Imaged with NICMOS", ApJ, **522**, L53.

II.3.1.2 - HR 4796A (A0V star, ~ 8 Myr)

HR 4796A's large thermal infrared excess implicated the existence of a significant amount of circumstellar dust close to the star (Jura 1991; Jura et al 1995). This was confirmed by modeling of mid-IR imaging observations of the thermally emissive grains by Koerner et al (1998) and Jayawardhana et al (1998). Attempts at imaging light scattered by debris particles, however, been unsuccessful until NICMOS and earlier attempts had produced negative results. For example, a non-detection was reported after K' observations at two epochs by Moulette et al (1997) using a stellar coronagraph on the COME-ON-PLUS/ADONIS AO (Beuzit et al 1997) system on the ESO 3.6-meter telescope at La Sille using 0.4" and 1" radius occulting masks to a stated sensitivity level of K = 20 mag arcsec^{-2}. Shortly thereafter, from single-orbit observations obtained in March and August 1998, NICMOS imaged the debris particles (in two spectral bands) which were seen to be confined to a very bright ring ~ 70 AU (1.05") in radius and within a region < ~ 17 AU wide (Schneider et al., 1999), possibly indicative of confinement by interactions with unseen co-orbital bodies of planetary mass.

Following the NICMOS observations, now with a foreknowledge of the debris system's morphology, geometry, and photometric properties, Augereau et al (1999) re-analysed the COME-ON-PLUS ADONIS images and reported a positive result from the same data set obtained by Moulette et al 1997.

In Figure 15 we compare the NICMOS PSF-subtracted F110W image with the ADONIS AO K' image as reprocessed by Augereau et al, which thus far remains the only published ground-based image of the HR 4796A debris disk in scattered light. Though, post-priori, the re-determined surface brightness of the disk at the radial distance of the ansae (just beyond the numerical mask used in the re-analysis) is in rough agreement (on the azimuthal average) with the NICMOS data (~ 12.2 mag arcsec^{-2}), significant differences remain in the structure of the disk and its flux densities elsewhere in the reprocessed ADONIS AO image. Second epoch NICMOS observations, at a substantially different spacecraft roll angle, and subsequent higher spatial resolution STIS imagery (Schneider 2002) confirmed results from the first epoch NICMOS observations.

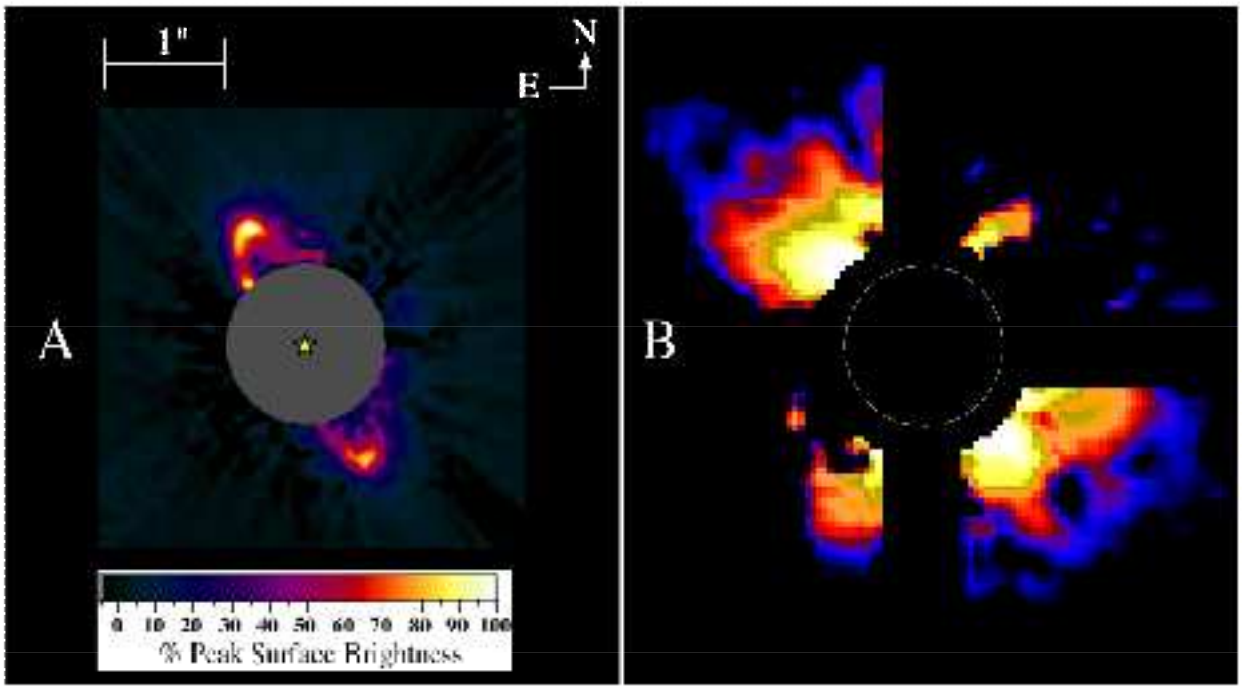

Figure 15. NICMOS (A) and COME-ON-PLUS/ADONIS ESO 3.6m+AO (B) PSF-subtracted coronagraphic images of the HR 4796A circumstellar debris disk.

References:

Augereau, J. C., Lagrange, A. M., Mouillet, D., Papaloizou, J. . B. & Grorod, P. A., "On the HR 4796 A Circumstellar Disk", 1999, A&A, **348**, 557

Beuzit, J.-L., Mouillet, D., Lagrange, A.-M. & Paufique, J., 1997, "A stellar coronograph for the COME-ON-PLUS adaptive optics system", A&A, **125**, 175

Jayawardhana, R., Fisher, S., Hartmann, L., Telesco, C., Pina, R. & Fazio, G., 1998, ApJ, **503**, L79

Jura, M., 1991, "The dust debris around HR 4796", ApJ, **383**, L79

Jura, M., Ghez, A. M., White, R. J., McCarthy, D. W., Smith, R. C. & Martin, P. G., 1995, "The fate of the solid matter orbiting HR 4796A" ApJ, **445**, 451
Koerner, D. W., Ressler, M. E., Werner, M. W. & Backman, D. E.,1998, "Mid-Infrared Imaging of a Circumstellar Disk around HR 4796: Mapping the Debris of Planetary Formation", ApJ, **503**, L83
Mouillet, D., Lagrange, A.-M., Beuzit, J.-L. & Renaud, N, 1997, "A stellar coronograph for the COME-ON-PLUS adaptive optics system. II. First astronomical results." A&A, **324**, 1083
Schneider, G., Smith, B. A., Becklin, E. E., Koerner, D. W.; Meier, R., Hines, D. C., Lowrance, P. J., Terrile, R. J., Thompson, R. I., Rieke, M., 1999, "NICMOS Imaging of the HR 4796A Circumstellar Disk", **513**, L127
Schneider, G., 2002, "High Contrast Imaging and the Disk/Planet Connection" Conference Proceesings: Hubble's Science Legacy: Future Optical-UV Astronomy From Space", ed. C. Blades, (ASP Conf Series), in press.

II.3.1.3 - TW Hya (K7V cTTS, ~ 5 Myr)

TW Hydrae possesses a large (230AU, 3.5" radius) nearly face-on optically-thick circumstellar disk first seen by NICMOS (Weinberger et al 1999, Weinberger et al 2002). The disk was effectively probed from a distance of 20 AU (~0.3") from the star to its outer extent with single-orbit (1260s total integration time) observations obtained coronagraphically in both the F110W and F160W filters. The disk was found to be extremely bright (21.6 ± 2.2 mJy in H-band = 11.7 mag from 0.38" < r < 4"), but unlike HD 141569A and HR 4796A, TW Hya appears relatively featureless with a fairly smooth radial brightness profile. These characteristics make TW Hya less of a contrast challenge then the debris disks previously discussed, e.g., with an order of magnitude higher in surface brightness than the brightest part of the HD 141569A disk at comparable radial distances from its central star. Measurements of the radial dependence of the surface brightness of this centrally cleared flared disk were found to be rather complex (Figure 16, left). These observations were independently confirmed with HST/WFPC-2 (Krist et al 1999, and later ,with HST/STIS (Schneider et al 2000).

The TW Hydrae disk was subsequently observed with ground-based H-band coronagraphy by Trilling et al 2001 on the IRTF with NSFCAM (Rayner et al 1993; Shure et al 1994)+CoCo (the Cold Coronagraph: Toomey et al 1998) on a night with 0.8" natural seeing. The IRTF coronagraphic images were obtained with a Gaussian-apodized (50% half-power) 1.86" diameter focal plane mask and articulating pupil plane mask in a series of eight exposures yielding a final (combined) 1620s image. Similar observations of a bright PSF reference star were made immediately after TW Hya. The CoCo observations trace the disk to an inner radius of 0.9" (60 AU), at the edge of its occulting mask, about 3 times further from the star than the limiting inner instrumental radius in the NICMOS images. To first order, the morphology of the CoCo image agrees with NICMOS in the spatial region of overlap, but in detail there are significant disparities in the disk photometry. In H-band the surface brightness at r = 1" (near the CoCo inner radius) was

measured by NICMOS as 1 mJy arcsec^{-2} and falling off as falling off as $r^{-2.6\pm0.1}$ from 45 to 150 AU, as was similarly found from independent HST WFPC-2 and STIS observations. The IRTF/CoCo measured surface brightness at r = 1" six times higher and falling off as $r^{-3.3\pm0.3}$ (as shown, comparatively, in Figure 16 right). The disparity highlights the difficulties in achieving photometrically reliable results in the face of temporally unstable PSFs, which can easily bias (ground-based) PSF-subtracted coronagraphy.

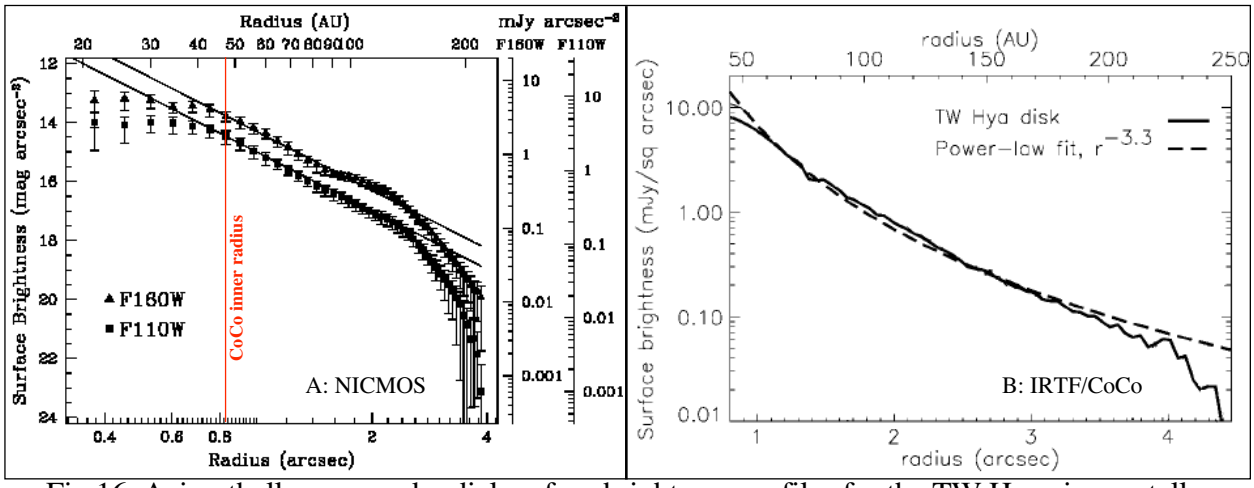

Fig 16. Azimuthally averaged radial surface brightness profiles for the TW Hya circumstellar disk as measured by NICMOS (left) from 20 AU outward and IRTF/CoCo (right).

References:

Krist, J. E., Stapelfeldt, K. R., Burrows, C. J., Menard, F., & Padgett, D. L., 1999, "HST/WFPC2 Images of a Possible Face-On Disk Around TW Hydrae", BAAS, **31**, 935

Krist, J. E., Stapelfeldt, K. R., Menard, F., Padgett, D. L. & Burrows, C. J. "WFPC2 Images of a Face-on Disk Surrounding TW Hydrae",2000, ApJ, **538**, 793

Rayner, J. T., et al. 1993, Proc. SPIE, 1**946**, 490

Schneider, G., Hines, D. C., Silverstone, M., Weinberger, A. J., Becklin, E. E., Smith, B.A., 2000, "Dust to Dust: Evidence for Planet Formation?", in Astrophysical Ages and Time Scales, eds. T. von Hipple, N. Manset, C. Simpson, ASP Conf Series, 245, 121.

Shure, M., et al. 1994, Exp. Astron., 3, 239

Toomey, D. W., Ftaclas, C., Brown, R. H., & Trilling, D. 1998, Proc. SPIE, **3354**, 782

Trilling, D. E., Koerner, D. W., Barnes, J.~W., Ftaclas, C. & Brown, R. H., 2001, "Near-Infrared Coronagraphic Imaging of the Circumstellar Disk around TW Hydrae",ApJ, **552**, L151

Weinberger, A. J., Becklin, E. E., Schneider, G., Chiang, E. I., Lowrance, P. J., Silverstone, M., Zuckerman, B., Hines, D. C. & Smith, B. A., 2002, "Infrared Views of the TW Hydra Disk", ApJ, **566**, 409.

Weinberger, A. J., Schneider, G., Becklin, E. E., Smith, B. A. & Hines, D. C.,1999, "NICMOS Imaging of a Circumstellar Disk About TW Hydrae", BAAS, **31**, 934

II.3.1.4 - False Detections

Ground-based disk imaging has also led, unfortunately, to spurious, and controversial (un-confirmed) results, which have muddied the waters for imaging and studying circumstellar debris

disks. For example, a debris system around a solar-like star, unexpected from thermal infrared measures, was announced (ESO 2000) for the planet-bearing star ι Hor from ADONIS coronagraphic observations with the SHARP II camera on the ESO 3.6-meter telescope, only to be later retracted (August 2001) as "new observations were made to verify the basic assumption that the Point-Spread-Function remains unchanged for reference stars of slightly different brightness (within half a magnitude). They showed that substantial changes in the Point-Spread-Function of the ADONIS system can occur for reference stars in the brightness interval employed for the ι Horologii observations...The conclusion is clear: the presumed dust disk around iota Horologii is an artifact, resulting from an underestimation of the calibration uncertainties in this type of delicate observation." And, a similar disk was suggested for 55 Cnc, another planet-bearing solar analog, from ground-based coronagraphic observations by Trilling et al.1998, but could not be confirmed with more sensitive HST/NICMOS observations (Schneider et al 2002).

References:
European Southern Observatory 2000, Press Release **27/00** (13 October 2000)
Schneider, G., Becklin, E. E., Smith, B. A., Hines, D., Weinberger, A. J., & Silverstone, M., 2001, "NICMOS Coronagraphic Observations of 55 Cancri", AJ **121**, 525.
Trilling D. E. & Brown, R. H., 1998, "A Circumstellar Disk Around A Star With a Known Planetary Companion", Nature, **395**, 775.

II.3.2 - Polarimetry & High Contrast Imaging: "Nulling" Polarimetry

Polarimetry offers another avenue for high contrast imaging. In particular, the technique enables the polarized component of the emission to be isolated from the unpolarized component. The primary polarizing mechanism of interest in many astronomical cases (and certainly for circumstellar material) is dust scattering, which can produce 100% polarized light from single scattering at right angles. Since polarization is a (pseudo-) vector, the net polarization observed from an astronomical object is highly dependent of the scattering geometry and the resolution of the instrument. The latter effect, so-called beam dilution, can reduce the observed polarization to near zero, even though the polarization from scattering is actually 100%.

As an example, a face-on circumstellar debris disk (such as TW Hya) presents a nearly right-angle scattering geometry with respect to our line of sight (LOS). Light from the illuminating central star along the direct LOS will be unpolarized, and much brighter than light highly polarized by scattering from the disk. Viewed in total light, the central star will completely overwhelm the scattered emission, but in polarized light (in principle), only the disk would be visible, as long as it is well resolved. In real observations, however, diffracted and instrumentally scattered light from

central point source (i.e. the PSF) will contribute photon noise and limit the detection threshold. Obviously, the higher the resolution, the more sensitive the observations will be to the polarized, scattered light from the debris disk. This technique has been used from the ground using AO to successfully detect circumstellar debris with optically bright central sources (e.g. HD 169142: Kuhn et al 2001; LkHa 262: Potter 2001; GM Aur: Potter 2002, Figure 17A).

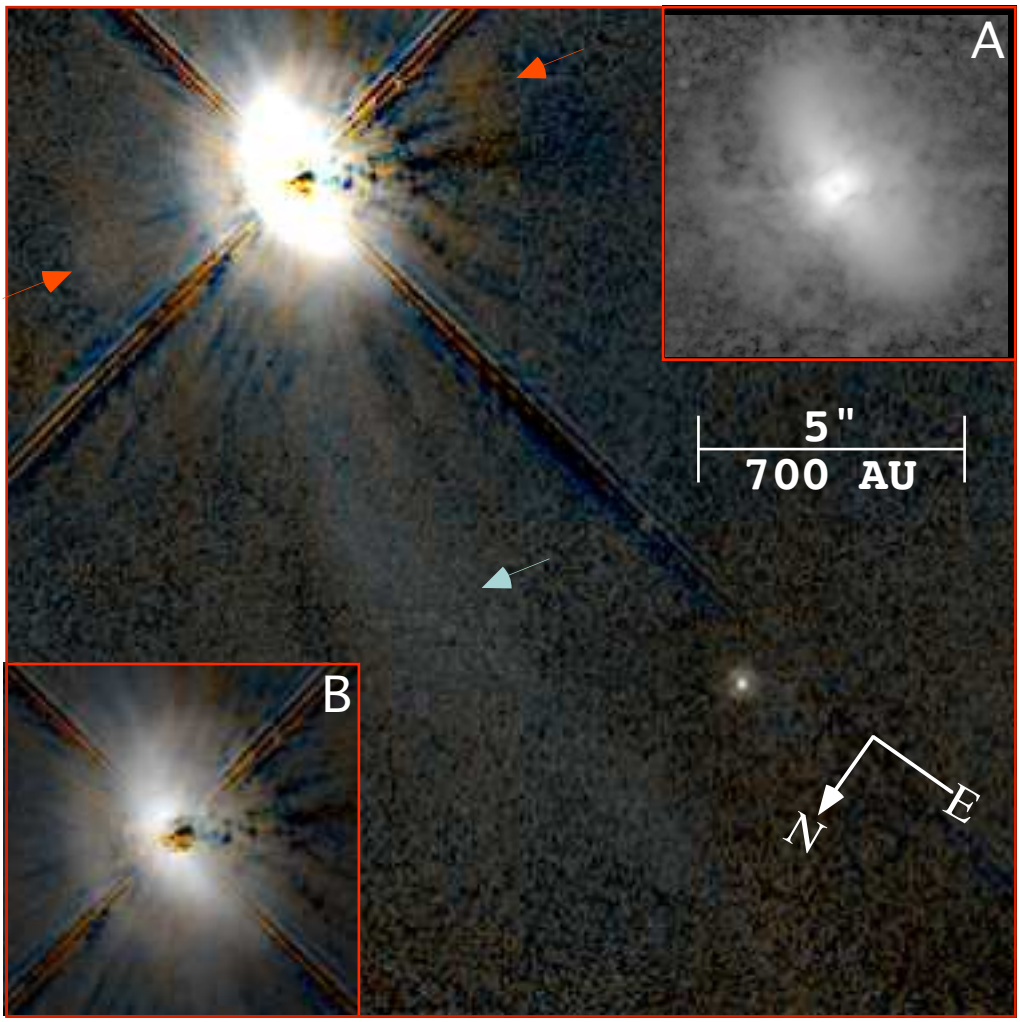

Figure 17. NICMOS coronagraphic PSF-subtracted F160W(blue) and F110W(red) composite image of GM Aur (Schneider et al 2003) alongside Gemini/Hokupa'a polarimetrically nulled H-band image (inset A) by Potter 2002. The disk flux densities in the Hokupa'a P*I image were scaled using the NICMOS flux calibration, and the region of the NICMOS field polarimetrically imaged with Hokupa'a (inset B) is shown at the same display stretch. NICMOS found two red polar lobes of likely (shocked?) outflow material with surface brightnesses of ~ 10 μJy arcsec^{-2}, which were undetected in the polarimetric image. Potter 2002 estimates that this material would have to be > 50% polarized to have been detectable in the P*I image. NICMOS also reveals a broad band of blue material to the NE of the disk.

For objects where the central source is obscured, AO will not work without LGS augmentation or anisoplanatic guiding, and only NICMOS can provide high resolution required

(e.g. CIT 6: Schmidt, Hines & Swift 2002). In addition, NICMOS provides a uniform PSF over the entire field of view, crucial for imaging low surface brightness objects without an AO beacon. For example, high resolution imaging polarimetry of the faint extended structure in the Egg Nebula (Sahai et al. 1998; Hines, Schmidt & Schneider 2000) is not currently possible with AO from the ground.

NICMOS delivers a unique imaging polarimetry capability. It is the only system that enables high-resolution polarimetry over a wide field (20" x 20") for objects that do not have a suitable AO beacon. For imbedded young stars, proto-planetary nebulae and active galaxies, NICMOS remains the most effective solution. Furthermore, combined coronagraphy and polarimetry with NICMOS promises to provide increased sensitivity for scattered light around (optically) obscured sources.

References:
Hines, D. C., Schmidt, G. D. & Schneider, G., 2000, "Analysis of Polarized Light with NICMOS", PASP, **112,** 983
Kuhn, J. R., Potter, D. & Parise, B., 2001, "Imaging Polarimetric Observations of a New Circumstellar Disk System", ApJ, **553,** L189
Potter, D., 2001, "Performance of a Dual Imaging Adaptive Optics Polarimeter", AAS Meeting **199**, #102.09.
Potter, D., 2002, Unpublished Communication (reported here)
Sahai, R., Hines, D. C., Kastner, J. H., Weintraub, D. A., Trauger, J. T., Rieke, M. J., Thompson, R. I.. & Schneider, G., 1998, "The Structure of the Prototype Bipolar Protoplanetary Nebula CRL 2688 (Egg Nebula): Broadband, Polarimetric, and H2 Line Imaging with NICMOS on the Hubble Space Telescope", ApJ, **492**, L163
Schmidt, G. D., Hines, D. C., & Swift, S. 2002, "The Nascent Bipolar Nebula Surrounding the Carbon-rich Variable CIT 6: Transition to Axisymmetry", ApJ, **576**, 429
Schneider, G., Wood, K., Silverstone, M., Hines, D. C., Koerner, D. W., Whitney, B. A., Bjorkman, J. E., and Lowrance, P. J., 2003. "NICMOS Coronagraphic Observations of the GM Aurigae Circumstellar Disk", ApJ, in press (to appear March 2003).

II.3.3 - Imaging Brown-Dwarf and Young Jovian Planet Companions

Direct detection of substellar companions (which appear as unresolved point sources) in the close environs of much-brighter stars by imaging techniques requires high-contrast capabilities and is dependent upon the in-band companion-to-star brightness ratio (usually expressed as ΔH or ΔK in the near-IR) and angular separation (ρ in arcseconds). Establishing instrumental detection limits for such objects, in principle, should be readily quantifiable in the ($\Delta H\{\Delta K\}$, ρ) phase-space, but in practice is difficult for ground-based systems because of the large temporal instabilities in AO performance (and the resulting PSF) due to variations in air-mass, wind-speed, seeing, etc. In general, of course, fainter (and thus less massive at the same age) and angularly closer companions are much more difficult to detect. Brown (L and T) dwarf (of 13–80 Jupiter masses) and gas-giant planet companions cool with age, approximately, roughly as $t^{-1.2}$ (Burrows et al 1997; Figure 18)

and hence are preferentially detected and imaged while they are young (e.g. now-confirmed NICMOS-found companions to CD -33° 7795; Lowrance et al 1999 and HR 7329; Lowrance et al 2000). Additionally, their contrast is greatly improved in the near-IR, where they are self-luminous, rather than seen by reflected starlight in the optical.

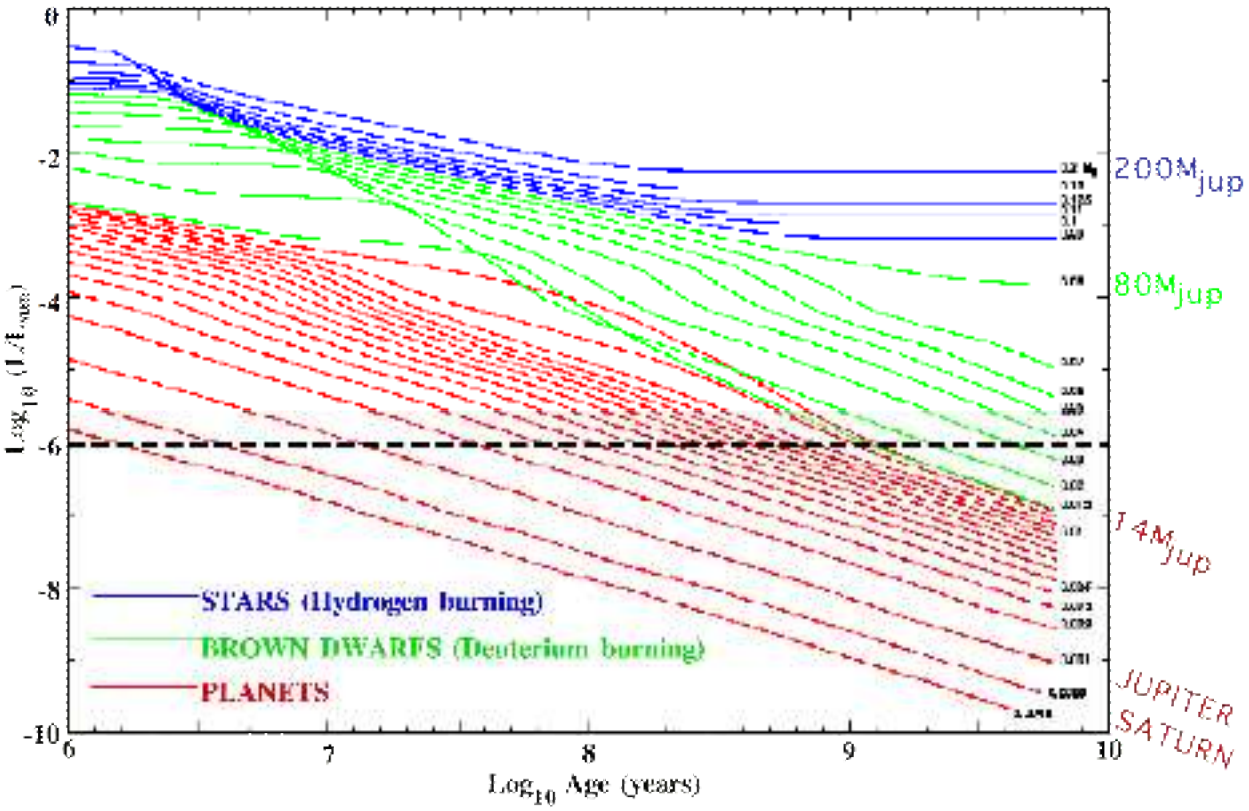

Figure 18. Detection space (above dashed line) for substellar companions by NICMOS PSF-subtracted coronagraphic imaging. (Adapted from Burrows et al 1997)

Brown dwarf companions at ages of ~ 100 Myr (bolometric luminosity ratios on the order of 10^{3-4}) pose no challenge for NICMOS at separations of ~ 1". Giant planets at comparable separations are more difficult, though at 10 My (such as the canonical or younger ages for members of the young associations of TW Hya, Chameleon, Horologium and β Pictoris in the southern hemisphere) objects with masses as small as Jupiter's can be detected at r = 2", and at 1 Myr at r = 1".

The ability to detect faint point sources near bright objects is enhanced by the instrumental reduction of background light from the central star. With NICMOS this is accomplished with a very high degree of repeatability to the levels noted in section II.3, by self-subtraction of the rotationally invariant PSF using the target star as its own PSF reference while rotating the field about the central star. Ground-based systems seek to improve on image contrasts by peaking up the

light of the central star (and any companions in the field) with adaptive optics, sometimes coupled with coronagraphic imaging systems, thus with AO correction, are dependent on the instantaneous state of the atmosphere.

In assessing the effectiveness of an instrumental system for high-contrast companion detection, traditional sensitivity measures often adopted significantly underestimate the limiting effects of non-random systematics and assume that the "noise", as expressed as a pixel-to-pixel variance, of the uncompensated background is both random and spatially uncorrelated. With such an assumption one expects an improvement in statistical sensitivity (i.e. S/N) with the square root of the integration time under a fixed photometric extraction aperture. This assumption breaks down, however, when instrumental artifacts are induced over multiple pixel scales, and is conflated when such artifacts have spatial frequencies on similar scales as the "signal" which is being sought. Such spatially correlated noise dominates in the bright-wings of stellar PSFs, in the regions of interest being surveyed for faint, sub-stellar, companions. The simple statistical metrics, which are often invoked to compare different instrumental systems, and presumed to scale in some fashion with Strehl ratio, inevitably fall short of delivering a true representation of what, one can actually achieve in practice.

Studies with HST/NICMOS by Lowrance (2002) and Schneider and Silverstone (2002) demonstrate the importance of divorcing raw *sensitivity* measures, in the conventional sense, from a more germane *detectability* metric. Both found that in the presence of temporal instabilities and non-random noise sources it is necessary to sequentially implant and recover high-fidelity models of "artificial stars" into a sufficiently large sample of observed images to truly understand the detection limits of any instrumental system. This was assessed for HST/NICMOS from two-orientation PSF-subtracted coronagraphy with 50 stars of spectral types G–M. The systematic noise from imperfect PSF subtractions is azimuthally non-isotropic, as are both the inferred sensitivities and probabilistic detection limits. From these data a 50% probability of detection as a function of companion distance and brightness ratio from its host star was found to be:

$$\mathbf{\Delta H(50\%) = 9.7\pm0.3 + 2.1 \times \rho(separation)"},$$

assuming azimuthally random companion placement but with a 30° rotation in field orientation between two observations in a single spacecraft orbit. This was also cast in terms of achievable S/N ratio in photometric apertures fully enclosing the PSF core. Arbitrarily, from the same sample a S/N=25 was achieved as:

$$\mathbf{\Delta H(S/N=25) = 8.1\pm0.3 + 2.1 \times \rho"}.$$

HST/NICMOS PSF-subtracted coronagraphic imaging data are intrinsically more stable than ground-based AO augmented systems can currently produce. To our knowledge, however, similar noise implantation experiments to quantitatively assess the repeatability of companion detections have not been undertaken from very faint companion surveys conducted on large ground-based AO augmented telescopes. For example, faint companion surveys undertaken at the W.M. Keck (Macintosh et al 2001), and Gemini and Suburu (Siegler, Close & Freed 2003) observatories with AO systems on large telescopes rely on the presumed scalability of Strehl ratios to assess detection sensitivity in the face of temporally variable PSFs.

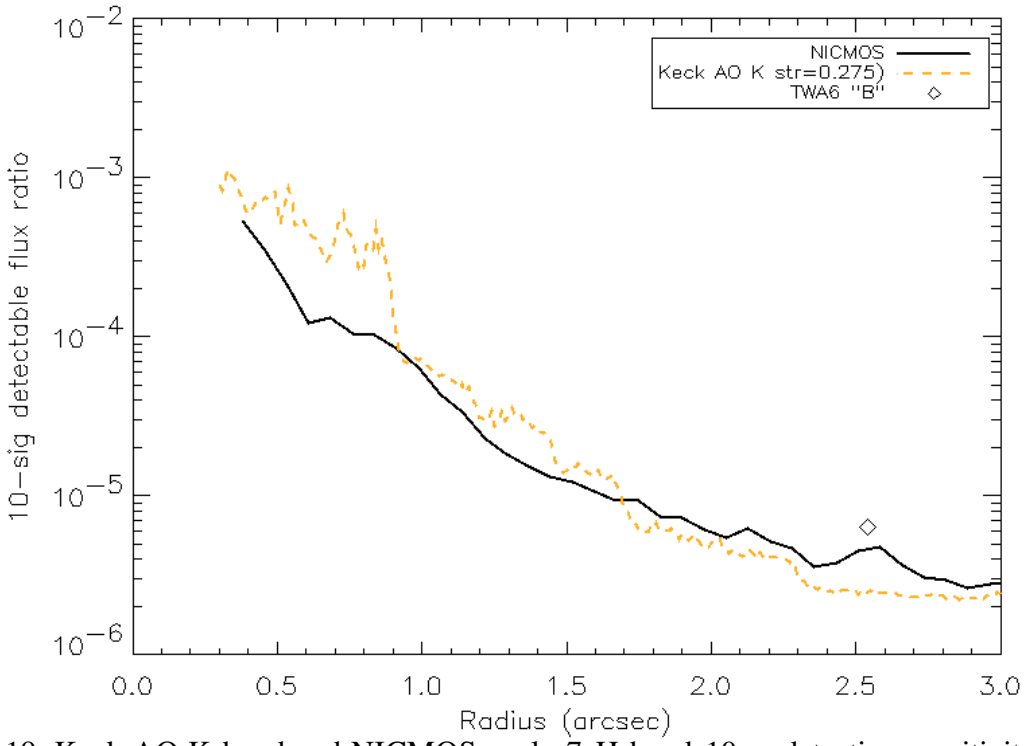

Figure 19. Keck AO K-band and NICMOS cycle 7 H-band 10 σ detection sensitivity curve from *uncorrelated* noise statistics. See text for improvement in NICMOS S/N with NCS-era quantum efficiency enhancement, and discussion of correlated noise.

Figure 19 reproduces such a *sensitivity* curve (10 σ noise variance) derived by Macintosh et al 2003 from Keck K-band companion survey images for a Strehl ratio of 0.28 (about 20% above the median over all observations in II.3.1), and is compared in a similar fashion to NICMOS cycle 7 H-band survey data. *In relative terms NICMOS is (at least) 2 to 5 time more sensitive than Keck AO in the critical region from 0.3" to 1.5,* the region around nearby young stars where Jovian planets are expected to be found. With its detectors now operating at 77K, NICMOS H-band quantum efficiency has increased by ~ 38% relative to Cycle 7. In PSF subtracted images (used in deriving Figure 19) the signal improves, with respect to the uncorrelated (pixel-to-pixel) noise, by

~ (1.95 S_{cycle7})/N. For stars of H > 6, observed with 2-orientation single-orbit PSF subtracted coronagraphy, this is improvement is fully realized in the r > 2" (in the region where Keck AO cannot control the diffuse halo of the primary PSF) as evidenced in Figure 24. Such representations of performance based only on uncorrelated noise statistics tend to be over-optimistic for reasons discussed above, and we illustrate with the instructive case of TWA 6 in section II.3.3.1.

NICMOS coronagraphy is applicable in investigating binarity to a limiting inner radius of ~ 0.3" from an occulted target because of the physical size of the coronagraphic "hole" at the first image plane of camera 2. Detection of low-mass companions at closer angular separations (and imaging diffuse material in these circumstellar regions), with NICMOS, must be done with direct imaging. PSF-subtraction alone provides significant contrast enhancement, as has been demonstrated, for example, by Low et al 1999 in the case of HD 98800 A/B (Figure 20).

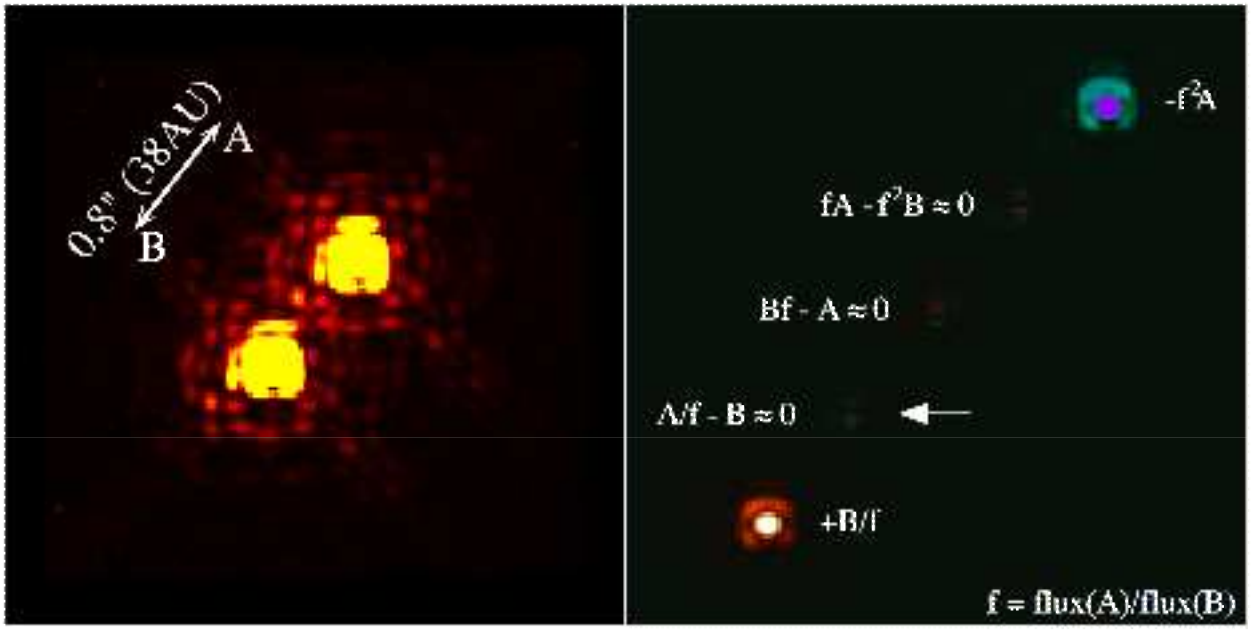

Figure 20. NICMOS Camera 1 replicate PSF subtraction of HD98800 A – B, using A as a template PSF for B[12]. Arrow indicates final PSF subtracted image.

Even without PSF-subtraction this domain of binary separations can be effectively explored with direct imaging even in low-mass systems as illustrated by Martin et al 1998 in the case of the binary brown dwarf CFHT-P1-18 (Figure 21, 0.045 and 0.035 solar masses) separated by 0.33".

This regime may also be explored with large-aperture ground-based AO systems, as discussed by Close et al 2003, and demonstrated with a curvature wavefront sensor with an

[12]http://nicmosis.as.arizona.edu:8000/AAS99_2/HD98800_POSTER.jpg

essentially zero read-noise avalanche photodiode (APD) on the Gemini north telescope. With this system, closed-loop AO correction was achieved on very low mass stars (V=18-20, I=14-16) producing ~ 0.1" FWHM images at K' (30% over the diffraction limit) with Strehl ratios of ~ 5% at R = 17 under good conditions (Siegler et al 2003). Figure 22 shows their AO detection of a R = 0.21", ΔH = 3.15 mag companion to LHS 2937 (I = 15.0) with a 150 mas FWHM AO corrected resolution. Three additional close binaries to very-low mass stars (LP4150-20, sp M7; 2M1750, sp M7.5; LP475-855, sp M7.5) in the separation range 0.119" – 0.294" with brightness ratios of ~ 2:1, were also reported by Close et al 2003. Such observations are complementary to deeper NICMOS coronagraphic surveys at separations > 0.3" (e.g. Schneider et al 2001).

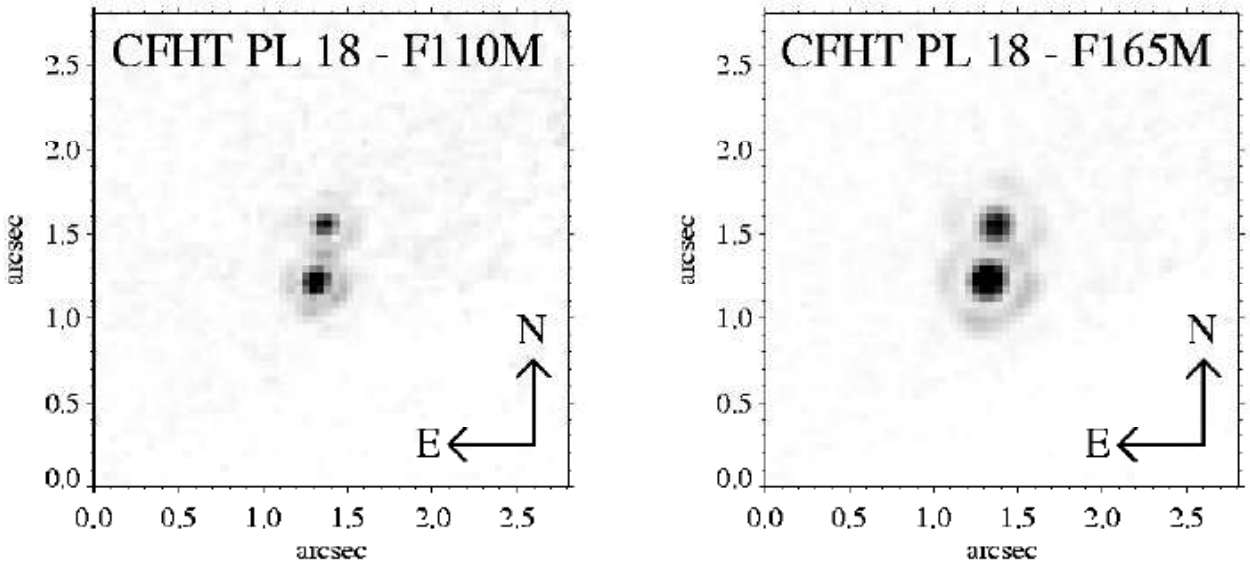

Figure 21. NICMOS Camera 1images of CFHT-P1-18 A/B.

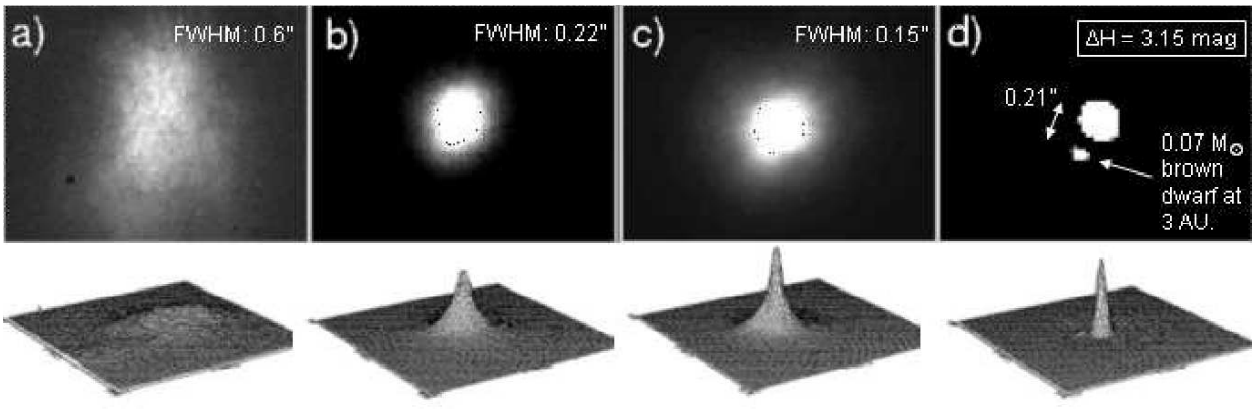

a) **AO off**; 3 combined 5-sec raw exposures.

b) **AO on**; 3 combined 5-sec raw exposures. Strehl has improved by a factor of 4.

c) **AO on**; 5 fully reduced 5-sec exposures with the best Strehl. Note companion at position angle 152° and narrower PSF.

d) **AO on**; low spatial frequencies removed from Figure c so as to fully reveal the brown dwarf companion[5].

Figure 22. Gemini AO imaging of LHS 2937A/B

The advent of curvature wavefront sensors with APDs permits ground-based AO telescopes to obtain AO closed-loop correction at fainter guide-star magnitudes then more "conventional" CCD Shack-Hartmann sensors (such as on the Keck AO system). Infra-red wavefront sensors will allow for the acquisition and AO correction on optically fainter, but redder stars. Presently though, as noted by Siegler et al 2003, there is only one large telescope with a working infrared wavefront sensor (VLT/UT4 with NAOS), and one large telescope with a zero-read noise wavefront sensor (SUBARU/AO). In either case obtaining AO correction for nearby brown dwarf primaries of spectral class ~ L3 and earlier is problematic on current systems and duplicity studies for such intrinsically cool (and faint) primaries remains in the domain of NICMOS. LGS equipped AO systems may push this envelope, but this still remains to be proven.

References:

Close, L. M., Siegler, N., Potter, D., 2003, "Adaptics optics guiding on very low mass and brown dwarf stars: who knew AO could go so low?", SPIE Conf. Ser., **4839**, in press.

Low, F. J., Hines, D. C., and Schneider, G., 1999, "NICMOS Observations of the Pre-Main-Sequence Planetary Debris System HD 98800", Astrophysical Journal, 520, L45.

Lowrance, P., McCarthy, C., Becklin, E., Zuckerman, B., Schneider, G., Webb., R., Hines, D., Kirkpatrick, J., Koerner, D., Low, F., Meier, R., Rieke, M., Smith, B., Terrile, R., and Thompson, R., 1999, "A Candidate Substellar Companion to CoD -33°7795 (TWA5)", Astrophysical Journal, **512**, L69

Lowrance, P.J., Schneider, G., Kirkpatrick, J.D., Becklin, E.E., Weinberger, A.J., Zuckerman, B., Plait, P., Malimuth, E.M., Heap, S.R., Schultz, A., Smith, B.A., Terrile, R.J., and Hines, D.C., 2000, "A Candidate Substellar Companion to HR 7329", Astrophysical Journal, **541**, L390

Lowrance, P.J., 2002, Ph. D. Thesis, UCLA

Macintosh, B. A., Brace, C. J., Carrano, C. J., Oliver, Patience, J., "High-contrast imaging with adaptive optics on the Keck Telescopes", SPIE Conf. Ser., **4839**, in press.

Martin. E. L., Basri, G., Brandner, W., Bouvier, J., Zapatero Osotio, M. R., Rebolo, R., Stauffer, J., Allard, F., Baraffe, I. & Hodgkin, S. T., "Discovery of a Very Low Mass Binary with th Hubble Space Telescope Near-Infrared Camera and Multiobject Spectrometer", ApJ, **509**, L113

Schneider, G., Becklin, E.E., Smith, B.A., Lowrance, P.J., Silverstone, M., NICMOS IDT/EONS Team, 2001, "A Coronagraphic Companion Survey of Nearby M-Dwarf Stars with HST/NICMOS", BAAS, AAS 198th Meeting, 77.17, and http://nicmosis.as.arizona.edu:8000/POSTERS/AAS_2001_JUNE_MDWARFS.JPG

Schneider, G., and Silverstone, M., 2002, "Coronagraphy with HST/NICMOS: detectability is a sensitive issue", Conference Proceedings: High-Contrast Imaging for Exo-Planet Detection, SPIE Conf. Ser., in press.

Siegler, N., Close, L. M & Freed, M., 2003 "Guiding on the Edge (V ~ 19): Results from an AO Survey of Very Low Mass Stars Searching for Extremely Faint Companions", SPIE Conf. Ser., **4839**, in press.

II.3.3.1 - The Illustrative Case of TWA 6

A faint point-like object was noted, even before PSF-subtraction, in NICMOS coronagraphic images of TWA6 (K 7V, H = 6.9, ~ 10 Myr member of the TW Hya association). Upon subtraction, a stellar-like (unresolved) object 200,000 times fainter than TWA6 ($\Delta H = 13.2$) appeared at an angular distance of 2.5" from the coronagraphically occulted star. The two

independent point-like images, each of S/N ~ 20, exhibit first Airy-ring structures, core profiles identical to point sources, and are rotated about the occulted target by the field re-orientation angle (of 30°). A recombination of the two-orientation difference image is shown in Figure 23 (left). The location of this object with respect to TWA6 was determined with a 1 σ uncertainty of 0.011" (even at this extreme contrast ratio), an important metric as putative companionship must be ascertained (or rejected) by differential proper motion measures. Because of the unavailability of NICMOS soon after this detection, an aggressive recovery program was conducted with the Keck AO system.

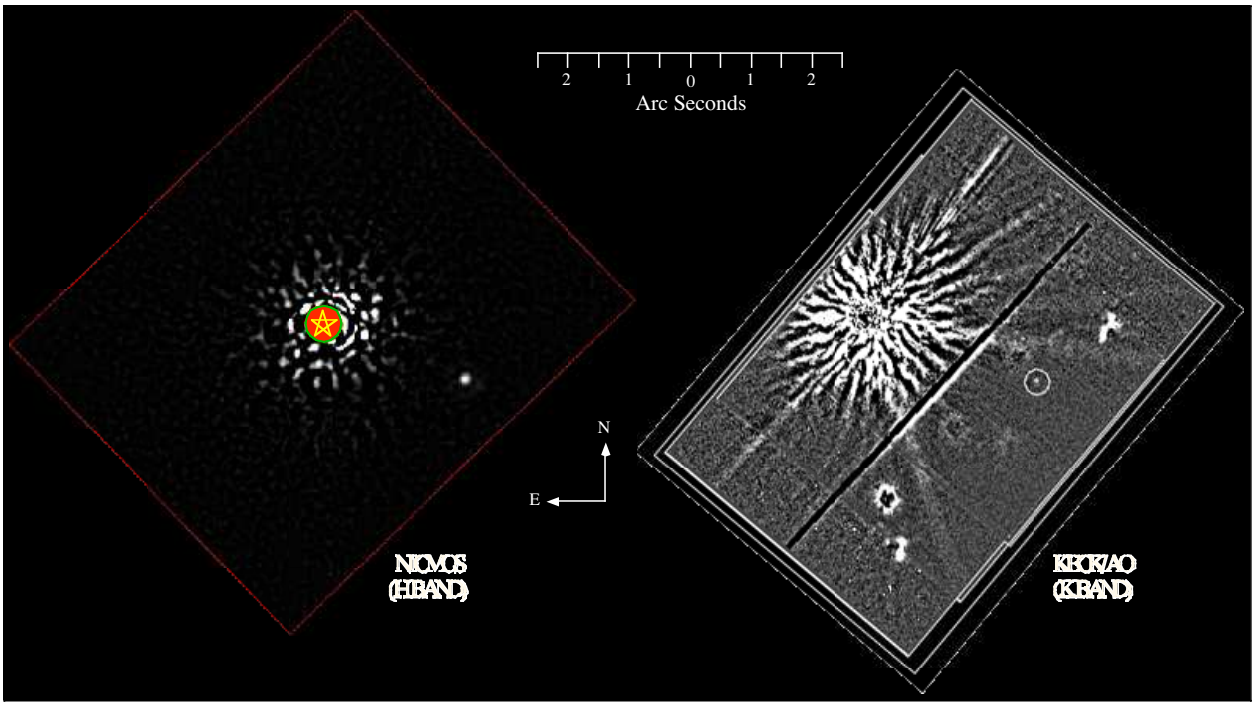

Figure 23. TWA6 field observed by NICMOS H-band(left) and Keck AO K-band (right) systems. The point-like object to the west of TWA6 is at a ΔH of 13.2 and separated by 2.5".

Figure 19 implies that the Keck AO system, even at this relatively large separation of 2.5", has sensitivity comparable to (or marginally better than) NICMOS. With a knowledge of the candidate companion's position and brightness from the NICMOS image, follow-up Keck imaging recovered the object (but likely would have produced a negative or questionable result without the NICMOS image for guidance). In nine attempts over several years, the object was undetectable four times (under conditions suitable for AO closed-loop correction). The first three detections with sufficient S/N to locate the object (e.g. Figure 23, right) resulted in ambiguous astrometric results (due to Strehl ratios of only ~ 5%). After four years (and a resulting proper motion of the primary of ~ 160 mas), on a subsequent attempt, an image was obtained with sufficient S/N to reject the conjecture of common proper motion. At nearly the same time, the restored NICMOS obtained a second-epoch

observation of the TWA6 field as its "first coronagraphic light" image (Figure 24) following SM3B.

Though taken BEFORE any post-servicing mission adjustments to the coronagraphic system (as part of a target acquisition re-enabling test) the image shown in Figure 24B yielded nearly identical image quality, sensitivity, and detectability as in HST cycle 7, with an identical astrometric uncertainty of 0.011".

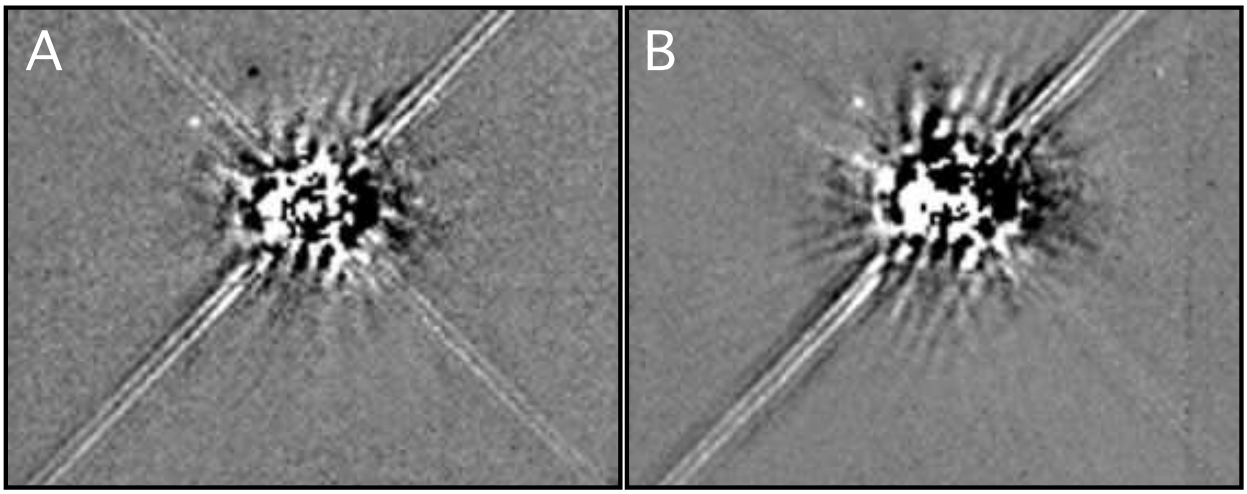

Fig 24. 30°-Rotated & PSF-subtracted coronagraphic images of the TWA6 field with $\Delta H = 13.2$ point source. A: Cycle 7 (–0.4 — +0.4 ADU/sec/pixel; 2.19 Jy/ADU/sec/pixel; $\rho = 2.56 \pm 0.011$) B: –0.55 — +0.55 ADU/sec/pixel; 1.59E-6 Jy/ADU/sec/pixel; $\rho = 2.36 \pm 0.011$") [Images displayed to same depth but have less pixel-to-pixel noise in B due to ~ 45% increase in detector QE].

References:

Burrows, A., Marley, M., Hubbard, W. B., Lunine, J. I., Guillot, T.; Saumon, D.; Freedman, R., Sudarsky, D., Sharp, C., "A Nongray Theory of Extrasolar Planets an Brown Dwarfs", 1997, ApJ, **491**, 856.

Lowrance, P., McCarthy, C., Becklin, E., Zuckerman, B., Schneider, G., Webb., R., Hines, D., Kirkpatrick, J., Koerner, D., Low, F., Meier, R., Rieke, M., Smith, B., Terrile, R., and Thompson, R., 1999, "A Candidate Substellar Companion to CoD -33°7795 (TWA5)", Astrophysical Journal, **512** , L69.

Lowrance, P.J., Schneider, G., Kirkpatrick, J.D., Becklin, E.E., Weinberger, A.J., Zuckerman, B., Plait, P., Malimuth, E.M., Heap, S.R., Schultz, A., Smith, B.A., Terrile, R.J., and Hines, D.C., 2000, "A Candidate Substellar Companion to HR 7329", Astrophysical Journal, **541**, L390.

Macintosh, B., Max, C., Zuckerman, B., Becklin, E., Kailser, D., Lowrance, P., Weinberger, A., Christou, J., Schneider, G., & Acton, S., 2001, "Keck AO Observations of TW Hydrae Association Members" in Young Stars Near Earth: Progress and Prospects, eds. R. Jayawarhadhana & T.P. Greene, ASP conf. Ser **244**, 309.

Macintosh, et al. , 2003, Spie Conf Ser., in press.

Siegler, N., Close, L. M. & Freed, M., 2002 "Guiding on the Edve (V ~ 19): Results from an AO Survey of Very Low Mass Stars Searching for Extreneely Faint Companions", SPIE Conf Ser., in press.

Schneider, G., 2003, "Coronagraphy with NICMOS", Conference Proceedings: The 2002 HST Calibration Worlshop, S. Arribas, A. Koekemoer, and B. Whitmore, submitted.

II. 4 - High Resolution Broad Band and Line Imaging

NICMOS cameras 1 and 2 achieve diffraction limited imaging with highest spatial resolutions in their shortest wavelength filters respectively, yielding a FWHM of 92 mas for the PSF of an unresolved (point) source under the pass band of the F095N ($\lambda c = 0.954\mu m$; 1%) filter and 106 mas for a spectrally flat source with the very broad F110W ($\lambda c = 1.000\mu m$; 54%) filter. These spatial resolutions scale linearly with wavelength. Camera 1, with 43 mas pixels, critically samples its PSF longward of 1μm (i.e. essentially for all of its filters), and camera 2 is critically sampled longward of 1.7μm. Camera 3, because of its marginal afocaliy, is not diffraction limited, but achieves spatial resolutions of ~ 0.2". With 200 mas pixels, camera 3 is undersampled by ~ a factor of two. Because of the very high degree of offset pointing precision and stability afforded by the HST pointing control system (both on the order of a few mas), enhanced PSF sampling is readily accomplished (and with low overheads for deep and narrow band imaging programs, where exposure times typically are on the order of minutes or longer) by "dithering" observations.

We illustrate the spatial resolving power of NICMOS with camera 2 (76 mas pixel) imaging of the prototypical and nearby ultraluminous infrared galaxy NGC 6240 obtained by Scoville et al 2000 in the broad band F110W, F160W and F222M (roughly J, H and K) filters, and van der Werf 1999 in red shifted H2 1-0 S(1). The broadband images (Figure 25) were dithered with four-position non-integral pixel offsets and recombined in processing onto a 2x finer grid for total integration times of 60s, 192s, and 224s, respectively. The neutral hydrogen line image (Figure 24, left panel) was (unfortunately) not dithered, but made by subtracting a median combination of six 512 s F215N (spectrally adjacent off-line continuum) images from a median combination of eight 512 s F216N (red shifted H2 1-0 S(1)) images.

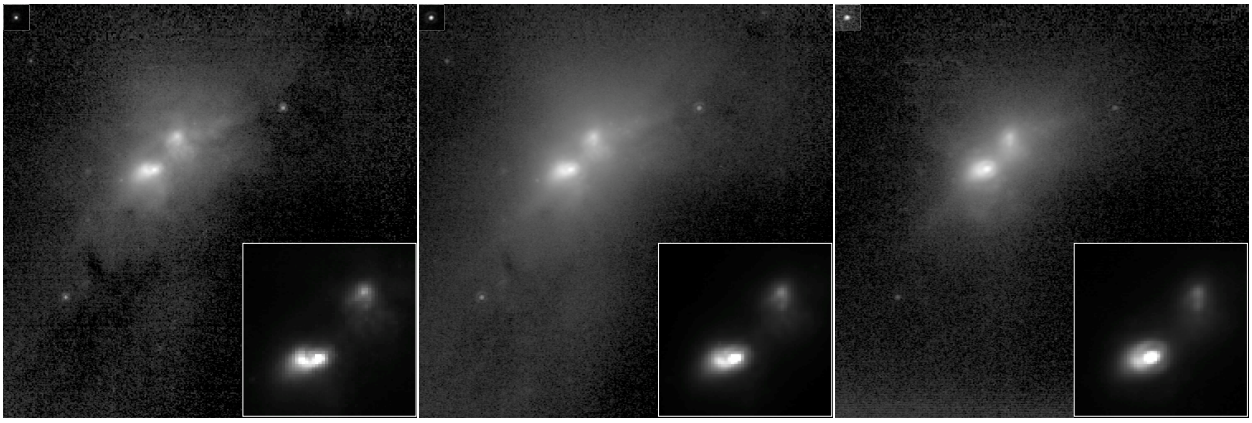

Figure 25. Left-to-right: NICMOS F110W, F160W, and F222M imaging of NGC 6240. Lower right insets of double nuclear region. Unresolved PSFs for each filter are shown in the upper left of each frame with contemporaneously measured FWHMs of 103, 144, and 181 mas, respectively.

The complex wavelength-dependent morphology of two nuclei (separated by ~ 1.6") and their circum-nuclear regions are resolved in these NICMOS images. Gerssen et al 2001 explained the Hα morphology of the southern nucleus as likely due to extinction. Lira et al 2002 noted that in WFPC-2 I-band (0.814mm) imaging, the northern (upper right in Figure 25) nucleus "is clearly resolved with a FWHM of ~ 0.23 arcsec", in agreement with the NICMOS F110W image. However, in the progression to K (through H) band, the morphology of the northern nucleus changes, and a second fainter component ~ 0.21" to the south is clearly seen in the NICMOS images.

It is clear from Table 3 that under favorable conditions large ground-based AO augmented telescopes are capable of outperforming HST+NICMOS in terms of spatial resolving power at similar wavelengths. As a comparative demonstration of capability we present K-band (similar pass band to NICMOS F222M) and H2 line imaging of the nuclear region NGC 6240 obtained with the Keck II AO system and NIRC2 camera (40 mas pixels) by C. Max alongside similarly stretched, scaled, and oriented NICMOS images (Figures 26 and 27, respectively).

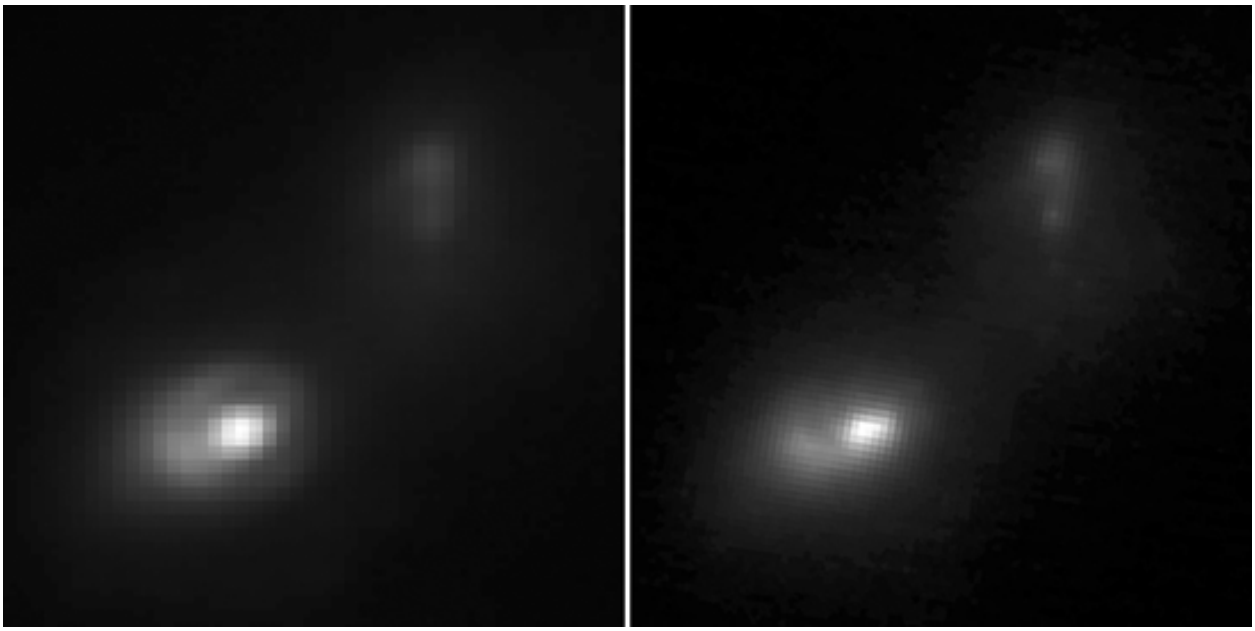

Figure 26. NICMOS F222M 224 s (left) and Keck AO/NIRC2 K-band 1080 s (right) images of the nuclei of NGC 6240.

NGC 6240 is an excellent AO demonstration target, and at $\delta = +2.4^{\circ}$ it transits the meridian at the Keck observatory at very low airmass. The Keck AO images were obtained while the natural seeing was excellent (0.32" in K-band) and acquired while the target was at airmass 1.05-1.07. The on-axis K-band Strehl ratio achieved with the V=13.5 guide star varied from 20-30% (a factor of two lower than suggested by Table 3, but commensurate with expectations based on measures by

MacIntosh as described in section I.6). AO correction for the guide star yielded a PSF FWHM of 120 mas x 160 mas (about a factor of 3 larger than suggested by Table 3), and 180 mas for the off-axis southern (brighter) nucleus. The PSF broadening is likely due to anisoplanatism, as the closest usable guide star was 35" from the nucleus (though it is possible that the nucleus is being resolved).

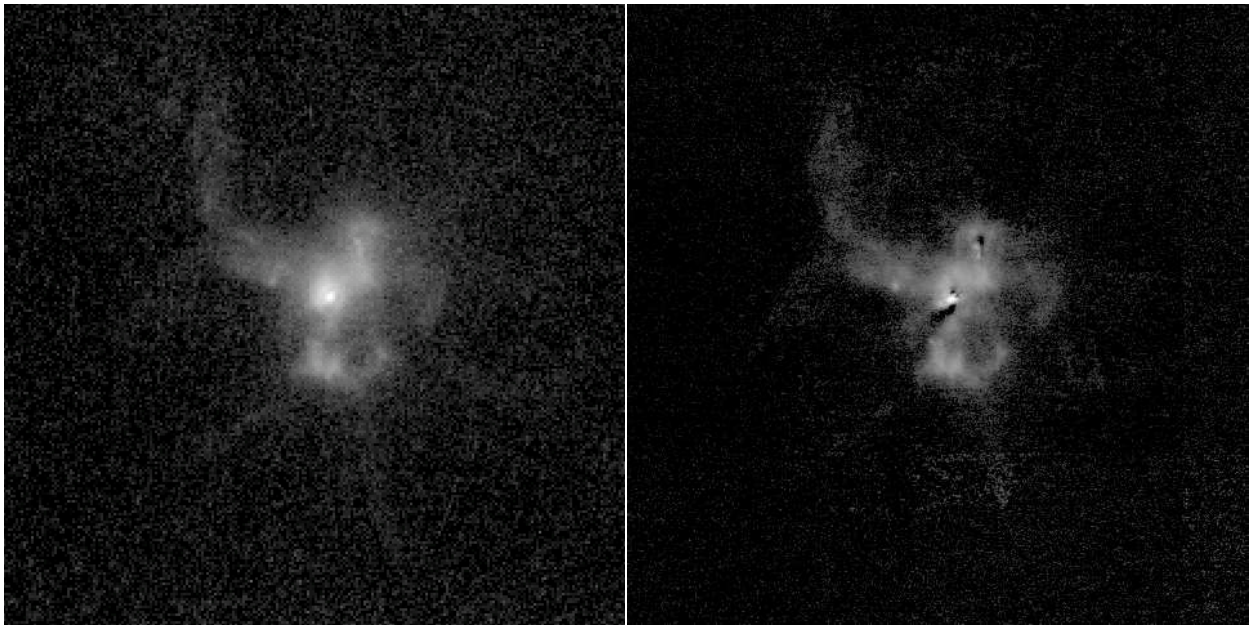

Figure 27. NICMOS 4096 s (left) and Keck AO/NIRC2 K-band 1200 s (right) continuum subtracted H2 1-0 S(1) line emission in NGC 6240.

The NICMOS and Keck AO F222M/K-band and H2 line images are qualitatively very similar, and we offer the following commentary:

(a) In both pass bands, virtually all of the features, both major and minor, are seen in both the NICMOS and Keck AO images, and have very similar appearance. The filamentary structures extending outward from the nuclear regions are in both images, as are the smaller knots and bubbles.

(b) The locations of all point-like features are the same.

(c) The Keck AO H2 image shows structural detail in the region between the nuclei (in the form of a curving "ribbon") which is not seen in the NICMOS image but, rather, is generally filled with emission. This may be because the Keck and NICMOS[13] filter pass bands differ.

(d) Continuum subtraction in the region of the nuclei in the Keck AO H2 image was corrupted due to temporal variations in the PSF structure between the "on" and "off" band

[13]http://nicmosis.as.arizona.edu:8000/FILTERS.html

images resulting in image artifacts (notably the black regions near the nuclei) which is not an issue in NICMOS imaging due to the high degree of temporal invariance of its PSF.

(e) The NICMOS "on" and "off" band H2 images discussed here, acquired in GO program 7882, were taken in a non-optimal manner, as they were not dithered. Dithering would not only better sample the PSF, but samples around bad pixels, and reduces the level of pixel-to-pixel instrumental noise. Dithering is a strategy highly recommended for such observations.

We have compared broadband images in K and (roughly equivalent) NICMOS/F222M pass bands, where wavelength-dependent AO correction is most effective (compared to J or H bands), and where dust extinction is less severe, and found very similar results. Because of the spectral invariance of the Strehl ratio for NICMOS, and hence linear improvement in achievable resolving power toward shorter wavelengths, for shorter (and multi) wavelength near-IR studies HST+NICMOS should be considered. For higher resolution imaging studies, HST's optical and UV imaging instruments can be employed. Panchromatic high-resolution imaging programs might be carried out most effectively in a complementary manner using large AO augmented ground-based telescopes at long near-IR wavelengths (and where the HST thermal background is large), NICMOS at shorter near-IR wavelengths, and STIS/ACS/WFPC-2 in the optical/UV.

Finally, we note that *spectroscopy* of the nuclear region of NGC 6240 with spatial resolution comparable to NICMOS and spectral resolution 2000-3000 in the regions of H-K bands have been obtained with the Keck AO system using NIRC2 (Bogdanovic et al 2001). Such spectroscopic observations cannot be carried out with NICMOS and lie solely in the domain of ground-based systems.

References:

Bogdanovic, T., Ge, J., Max, C. E., & Brandt, N. W., 2001, "Near-IR Imaging and Spectroscopy of NGC 6240 with Adaptive Optics", AAS Meeting **199**, 49.03

Scoville, N. Z., Evans, A. S., Thompson, R., Rieke, M., Hines, D. C., Low, F. J., Dinshaw, N., Surace, J. A., Armus, L., 2000, "NICMOS Imaging of Infrared-Luminous Galaxies", AJ, , 119, 991.

Gerssen, J., van der Marel, R.P., Axon, D.,J., Mihos, C., Hernquist, L., 2001, "HST Observations of NGC 6240"in ASP Conf Ser. **249**, 665.

Lira, P, Ward, M.J., Zezas, A., and Murray, S.S., "Chandra HRC and HST observations of NGC 6240: resolving the active galactic nucleus and starburst", MNRAS, **333**, 709.

Van der Werf, 1999, "H2 emission as a physical probe of the interstellar medium of starforming galaxies", in H2 in Space, Eds.: F. Combes, G. Pineau des Forets, Cambridge University Press, Astrophysics Series

SUMMARY

Adaptive optics systems can provide very substantial performance improvements on large telescopes relative to systems that are not so equipped. In particular, AO systems can deliver spatial resolutions at or approaching the theoretical instrumental diffraction limit of a telescope's optical system yielding, for telescopes larger than HST, superior resolving power at comparable near-IR wavelengths. For programs requiring raw resolving power, and where issues such as photometric efficacy and completeness and/or astrometric precision (particularly in crowded and obscured fields), image contrast and temporal stability are of less concern then suitably instrumented ground-based AO systems can provide the means to achieving such a goal. High spectral resolution near-IR spectrophotometry must be done utilizing ground-based facilities, as NICMOS provides only a low spectral resolution grism spectrophometric mode. For imaging programs requiring low backgrounds, a spatially invariant (field and pointing independent) and temporally stable and repeatable point spread function, very high contrast (with or without coronagraphy), and/or access to passbands hampered by atmospheric Telluric absorption (such as Paschen α) HST+NICMOS would likely be the platform of choice.

For many programs understanding systematic effects which dominate measurement uncertainties is paramount to success. The intrinsic optical stability and repeatability of the HST+NICMOS space-based imaging system removes many of the limiting uncertainties externally imposed on ground-based observations. Here we quote "A Note of Caution" offered to AO users by the W.M. Keck Observatory in their instructions to AO observers[14]: "The performance obtained with AO is a function of a number of factors including the magnitude and size of the guide star, the separation of the guide star from the science object, the seeing conditions (amplitude, speed and altitude of the turbulence), the distance from the zenith, telescope wind shake, and the sky brightness. There is no single number or plot that will tell you how well you will do on your science object. Observer's are therefore strongly recommended to keep in mind these varying conditions in preparing their proposals and observing plans. ***What might be possible on one night may not be possible on another night***. " We have emphasized he latter, as on a given AO system a successful observation under favorable conditions may not be a reliable predictor of more typical performance.

Variabilities in AO performance can be particularly detrimental for survey and search programs, where non-uniform survey incompleteness can (and does) lead to individual target false negatives (or false positives in the face of optical artifacts) and unduly biases sample statistics. A

[14]http://www2.keck.hawaii.edu:3636/realpublic/inst/ao/observing/observing.html

more prophitable strategy would be to conduct such targeted survey programs (e.g. damped Lyman α systems, circumstellar debris disks, young exosolar planets, companions to objects below the stellar main sequence, KBOs, asteroid binarity, SFR measurements [by Paschen α] of active galaxies, etc.) at low-risk and high efficiency with HST, with ground-based follow-up when possible once the new-found target characteristics have been established. For such follow-ups ground and HST based observations may be symbiotic where their domains of observability overlap, or expansive where they are not.

Advances in ground-based adaptive optics technologies continue. Multi-conjugate AO systems, more robust laser guide stars, even larger ground-based telescopes, and other enabling technologies hold promise to expand the domain of ground-based observations in the years (and decades) to come. In the interim, HST+NICMOS can fill the void and should be used advantageously while the recently revived NICMOS continues to function with its newly integrated (and thus-far completely successful) active cooling system. The continuance of NICMOS without curtailment beyond 2005 is not assured once the next generation power-hungry HST instruments are installed. We are at a critical juncture where the uniqueness space offered by HST+NICMOS can be used to great advantage until the domains of future ground and space near-IR systems someday obviate the need for NICMOS. But that, clearly, is not the state of near-IR observational astronomy today.

Acknowledgements. We have attempted to incorporate and present up-to-date information with regard to the state-of-the-art for AO augmented ground-based telescopes recognizing that such information is volatile and capabilities are evolving on timescales shorter than formal publications often appear. This report would not have been possible without the inputs, insights, and suggestions by many researchers actively engaged in HST and ground-based/AO observations. In addition to the previously noted formal contributors we wish to thank and acknowledge beneficial advice and commentary provided by Carol Grady(GSFC), Paul Kalas (UC Berkeley), Patrick Lowrance (IPAC), Russell Makidon (STScI), Alfred Schultz (STScI), Murray Silverstone (UofA), Bruce Woodgate(GSFC), and Ben Zuckerman (UCLA). We also wish to acknowledge the many people who have contributed to web-based information from which we have drawn, and have cited in footnotes throughout this report. Finally, we are particularly grateful to Steve Beckwith (Director, STScI) and Duccio Macchetto (Science Policies Division Head, STScI) for soliciting this report. We hope this report will serve as a useful adjunct to the Cycle 12 Time Allocation Committee evaluations in awarding NICMOS observing time. We recognize that by its very nature this summary report likely suffers from incompleteness, as it is intended to be representative and not all-

inclusive. We apologize for any unintended omissions and necessary brevity in any areas of particular interest to individual readers.

This work is based, in part, on observations with the NASA/ESA Hubble Space Telescope, obtained at the Space Telescope Science Institute, which is operated by AURA, Inc. under NASA contract NAS2-6555 and supported by NASA grants NAG5-3042 and NAG5-10843 to the NICMOS IDT.